



**HAL**  
open science

## Is there an effect of Bay of Bengal salinity on the northern Indian Ocean climatological rainfall?

K. S. Krishnamohan, Jérôme Vialard, Matthieu Lengaigne, Sébastien Masson, Guillaume Samson, Stéphane Pous, Suresh Neetu, Fabien Durand, S. S. C. Shenoi, Gurvan Madec

### ► To cite this version:

K. S. Krishnamohan, Jérôme Vialard, Matthieu Lengaigne, Sébastien Masson, Guillaume Samson, et al.. Is there an effect of Bay of Bengal salinity on the northern Indian Ocean climatological rainfall?. *Deep Sea Research Part II: Topical Studies in Oceanography*, 2019, 166, pp.19-33. 10.1016/j.dsr2.2019.04.003 . hal-02301498

**HAL Id: hal-02301498**

<https://hal.sorbonne-universite.fr/hal-02301498v1>

Submitted on 30 Sep 2019

**HAL** is a multi-disciplinary open access archive for the deposit and dissemination of scientific research documents, whether they are published or not. The documents may come from teaching and research institutions in France or abroad, or from public or private research centers.

L'archive ouverte pluridisciplinaire **HAL**, est destinée au dépôt et à la diffusion de documents scientifiques de niveau recherche, publiés ou non, émanant des établissements d'enseignement et de recherche français ou étrangers, des laboratoires publics ou privés.

# Accepted Manuscript

Is there an effect of Bay of Bengal salinity on the northern Indian Ocean climatological rainfall?

K.S. Krishnamohan, J. Vialard, M. Lengaigne, S. Masson, G. Samson, S. Pous, S. Neetu, F. Durand, S.S.C. Shenoi, G. Madec

PII: S0967-0645(18)30132-2

DOI: <https://doi.org/10.1016/j.dsr2.2019.04.003>

Reference: DSR II 4568

To appear in: *Deep-Sea Research Part II*

Received Date: 9 June 2018

Revised Date: 27 March 2019

Accepted Date: 1 April 2019

Please cite this article as: Krishnamohan, K.S., Vialard, J., Lengaigne, M., Masson, S., Samson, G., Pous, S., Neetu, S., Durand, F., Shenoi, S.S.C., Madec, G., Is there an effect of Bay of Bengal salinity on the northern Indian Ocean climatological rainfall?, *Deep-Sea Research Part II* (2019), doi: <https://doi.org/10.1016/j.dsr2.2019.04.003>.

This is a PDF file of an unedited manuscript that has been accepted for publication. As a service to our customers we are providing this early version of the manuscript. The manuscript will undergo copyediting, typesetting, and review of the resulting proof before it is published in its final form. Please note that during the production process errors may be discovered which could affect the content, and all legal disclaimers that apply to the journal pertain.



1                   **Is there an effect of Bay of Bengal salinity on the Northern Indian Ocean**  
2                   **climatological rainfall?**  
3

4  
5                   KS. Krishnamohan<sup>1</sup>, J. Vialard<sup>1</sup>, M. Lengaigne<sup>1,2</sup>, S. Masson<sup>1</sup>, G. Samson<sup>3</sup>, S. Pous<sup>1,6</sup>,  
6                   S. Neetu<sup>4</sup>, F. Durand<sup>3</sup>, S.S.C Shenoi<sup>5</sup>, G. Madec<sup>1</sup>  
7

8  
9                   <sup>1</sup> Sorbonne Universités (UPMC, Univ Paris 06)-CNRS-IRD-MNHN, LOCEAN Laboratory, IPSL, Paris, France

10                   <sup>2</sup> Indo-French Cell for Water Sciences, IISc-NIO-IITM-IRD Joint International Laboratory, NIO, Goa, India

11                   <sup>3</sup> IRD/Laboratoire d'études en Géophysique et Océanographie Spatiales (LEGOS), Toulouse, France

12                   <sup>4</sup> National Institute of Oceanography, Goa, India.

13                   <sup>5</sup> Indian National Centre for Ocean Information Services, Hyderabad, India

14                   <sup>6</sup> Department of Oceanography, University of Cape Town, South Africa  
15  
16  
17  
18  
19  
20

21                   Corresponding author:

22                   Krishnamohan K.S

23                   LOCEAN - Case 100

24                   Case 100 - Université P. et M. Curie

25                   4, Place Jussieu - 75252 Paris Cedex 05

26                   FRANCE

27                   Email: krishmet@gmail.com  
28

29  
30  
31  
32  
33  
34  
35  
36  
37  
38  
39  
40  
41  
42  
43  
44  
45  
46  
47  
48  
49**Abstract**

The northern Bay of Bengal (BoB) receives a large amount of freshwater directly from monsoonal rains over the ocean, and indirectly through river runoffs. It has been proposed that the resulting strong salinity stratification inhibits vertical mixing of heat, thus contributing to maintain warm sea surface temperature and high climatological rainfall over the BoB. In the present paper, we explore this positive feedback loop by performing sensitivity experiments with a 25-km resolution regional coupled climate model, that captures the main BoB features reasonably well. We confirm that salinity stratification tends to stabilize the upper ocean, thereby increasing the mixed layer warming due to vertical mixing by  $\sim +0.5^{\circ}\text{C}\cdot\text{month}^{-1}$  on annual average. Salinity however also induces a compensating cooling by altering the mixed layer heating rate by air-sea heat fluxes, so that the net effect on climatological surface temperature is negligible. During and shortly after the southwest monsoon, this compensation predominantly occurs through increased cooling by upward latent heat fluxes. During boreal winter, it occurs because salinity favours a thinner mixed layer, which is more efficiently cooled by negative air-sea heat fluxes. These compensations result in a negligible climatological surface temperature and rainfall change at all seasons. This weak influence of salinity stratification on climatological surface temperature and rainfall in our model is robust when applying a flux correction to alleviate model biases, when neglecting the solar absorption below the mixed layer and when using different atmospheric radiation and convective parameterizations.

## 50 1. Introduction

51 With 60% of jobs in the agriculture sector, the livelihood of the densely-populated Indian  
52 subcontinent crucially depends on the Indian summer monsoon rainfall (Webster et al., 1998;  
53 Gadgil and Gadgil, 2006), which accounts for about 90% of annual precipitation over India.  
54 During boreal summer, the differential heating between the Asian landmass and the ocean to the  
55 south sets up a low pressure area over south Asia reinforced by the elevated heating on the  
56 Tibetan plateau (Li and Yanai, 1996). The dynamical response to this pressure gradient consists  
57 of a low-level and large-scale cross-equatorial flow (Joseph and Raman, 1966; Findlater, 1969),  
58 which induces surface evaporation and collects moisture over the Indian Ocean. From June to  
59 September, the northern branch of this flow results in strong southwesterly winds over the  
60 Arabian Sea (AS) and the associated moisture transport is then flushed over the Indian  
61 subcontinent and Bay of Bengal (BoB) (Findlater, 1969).

62 This strong south-west monsoon rainfall and the associated larger riverine input (mainly  
63 from the Ganges-Brahmaputra and Irrawaddy) results in a large freshwater input into the BoB  
64 during the southwest monsoon, with rainfall accounting for more than two thirds (e.g. Sengupta  
65 et al., 2006; Akhil et al., 2014; Chaitanya et al., 2014). This large freshwater input into a  
66 relatively-small, semi-enclosed basin yields some of the lowest climatological Sea Surface  
67 Salinities (SSS) in the tropical band (Chaitanya et al., 2014), with a maximum freshening in the  
68 top 10-40 meters, resulting in a sharp near-surface salinity stratification, especially in the  
69 northern BoB (e.g. Vinayachandran et al., 2002; Behara and Vinayachandran, 2016; Sengupta et  
70 al., 2016). This salinity stratification has a strong stabilizing effect on the upper ocean,  
71 maintaining a shallow mixed layer (Mignot et al., 2007; Girishkumar et al., 2013) and often  
72 resulting in the formation of a barrier layer, i.e. a salinity-stratified layer between the bottom of  
73 the mixed layer and top of the thermocline (Lukas and Lindstrom, 1991; Sprintall and Tomczak,  
74 1992). Barrier layers usually appear during summer in the eastern BoB and mature during winter  
75 both in amplitude and spatial extent, covering the entire northern BoB (Rao and Sivakumar,  
76 2003; Thadathil et al., 2007; Kumari et al., 2018; Li et al., 2017).

77 The barrier layer impacts the mixed layer temperature heat budget, by isolating the warm  
78 surface layer from the colder upper thermocline and preventing the entrainment of cold  
79 subsurface water into the mixed layer (Vialard and Delecluse, 1998). The salinity stratification  
80 within the barrier layer can even support temperature inversions (i.e. warmer water below than  
81 within the mixed layer, e.g. Han et al., 2001; Girishkumar et al., 2013; Thadathil et al., 2016). In

82 presence of such temperature inversions, entrainment (that usually cools the mixed layer) can  
83 even warm the surface layer during winter (de Boyer Montegut et al., 2007). The strong salinity  
84 stratification thus appears to play a key role in maintaining a relatively high Sea Surface  
85 Temperature (SST) in the BoB by reducing the vertical mixing of heat during and after the  
86 southwest monsoon (de Boyer Montegut et al., 2007).

87 In a seminal study, Shenoi et al. (2002) proposed that the vertical salinity stratification in  
88 BoB could contribute to a coupled ocean-atmosphere positive feedback loop that maintains  
89 intense climatological rainfall regionally. In this hypothesis, summarized on the sketch of Fig. 1,  
90 a strong rainfall and river freshwater forcing yields a low SSS and strong vertical salinity  
91 stratification in the BoB (Step I on the Fig. 1). This strong, stable salinity stratification (and the  
92 associated barrier layer) inhibits the cooling of the mixed layer by turbulent mixing at its bottom,  
93 maintaining SST above 28.5°C during the entire summer monsoon (Step II on Fig. 1). Such SST  
94 above 28.5°C is a necessary condition for deep atmospheric convection to occur (Gadgil et al.,  
95 1984; Graham and Barnett, 1987), thus allowing to maintain regional rainfall and runoffs (Step  
96 III on Fig. 1) and completing the feedback loop. Shenoi et al. (2002) supported this hypothesis by  
97 the analysis of observational climatologies, that indicate that the available mixing energy from  
98 the wind is not sufficient to overcome the stabilizing effect of the salinity stratification. The  
99 feedback loop proposed by Shenoi et al. (2002) could thus contribute to maintain a high  
100 climatological rainfall over the BoB.

101 The Shenoi et al. (2002) hypothesis is not only important to understand the present-day  
102 BoB climatological rainfall, but may also be very relevant in the context of anthropogenic climate  
103 change. Climate models and theoretical arguments indeed support an intensification of the  
104 hydrological cycle as the troposphere warms in response to increasing greenhouse gases  
105 concentrations (e.g. Held and Soden, 2006). The observational records already detect an  
106 intensification of salinity contrasts as a result, *i.e.* increasing salinities in regions dominated by  
107 evaporation, and decreasing salinities in high rainfall regions, including in the BoB (e.g. Durack  
108 and Wijfels, 2010). The Shenoi et al. (2002) hypothesis, if correct, would provide an additional  
109 positive feedback mechanism to further enhance the climate change impact on rainfall regionally  
110 in the Bay of Bengal region. This provides an additional motivation to investigate the validity of  
111 this hypothesis thoroughly.

112 Ocean modelling experiments have explored the consequences of the BoB salinity  
113 stratification before (Han et al., 2001; Howden and Murtugudde, 2001; Behara and

114 Vinayachandran, 2016). Han et al. (2001) used a reduced-gravity ocean model and found that the  
115 effect of freshwater fluxes was dominated by the effect of river runoffs and resulted in a localised  
116  $\sim 0.5\text{-}1^\circ\text{C}$  surface warming in the northwestern BoB in summer, in response to the Kelvin wave  
117 forced by the Ganges-Brahmaputra river inflow. Howden and Murtugudde (2001) used a reduced  
118 gravity primitive equation model and only found a very local impact of river discharge on BoB  
119 summer SST, confined to nearest grid points to the Ganges-Brahmaputra and Irrawady river  
120 mouths, and more widespread  $\sim 0.5^\circ\text{C}$  cooling in the northeastern BoB during winter. In a recent  
121 study using an ocean general circulation model, Behara and Vinayachandran (2016) found that  
122 freshwater fluxes induced a  $\sim 0.5^\circ\text{C}$  warming in the northwestern BoB during summer, and 0.5 to  
123  $1.5^\circ\text{C}$  cooling in the eastern BoB during both summer and winter.

124 None of the studies above however represents deep atmospheric convection explicitly, a  
125 key element in the Shenoi et al. (2002) hypothesis (Fig. 1). A recent study with a coupled general  
126 circulation model (Vinayachandran et al., 2015) suggests that river runoffs contribute to a 10%  
127 decrease of Indian summer rainfall, opposite to what should be expected from Shenoi et al.  
128 (2002) hypothesis. This study however switched off river runoffs not only in the BoB but at a  
129 global scale, and finds really modest SST changes in the BoB ( $\sim 0.2^\circ\text{C}$ ). It is therefore possible  
130 that the Indian monsoon change in this study is rather associated with the remote response to  
131 large SST signals in the northern Pacific and Atlantic Ocean ( $>2^\circ\text{C}$ ). The most relevant coupled  
132 model study of the Shenoi et al. (2002) hypothesis is thus that of Seo et al. (2009), using a fully  
133 coupled regional circulation model. This study mimics freshwater fluxes into the BoB by  
134 applying a relaxation to SSS climatology, which makes the SSS much lower in the BoB as  
135 compared to their reference experiment. This increased salinity stratification however resulted in  
136 a very weak salinity-induced surface warming in the northwestern BoB in summer ( $\sim 0.2^\circ\text{C}$ ), and  
137 a weak atmospheric response.

138 So far, the hypothesis of Shenoi et al. (2002) is thus not clearly supported by existing  
139 numerical experiments. On the one hand, ocean modelling studies (Han et al., 2001; Howden and  
140 Murtugudde, 2001; Seo et al., 2009; Behara and Vinayachandran, 2016) do not resolve potential  
141 atmospheric feedbacks associated with deep atmospheric convection changes. On the other hand,  
142 existing coupled model studies find rainfall changes that are either negligible (Seo et al., 2009) or  
143 opposite to what is expected from the Shenoi et al. (2002) hypothesis (Vinayachandran et al.,  
144 2015). For these reasons, we aim to revisit this hypothesis using a state-of-the-art regional  
145 coupled model that captures the main features of the Indian Ocean mean climate, including the

146 monsoon, and its time-variability (Samson et al., 2014). We will do so by comparing reference  
147 experiments with sensitivity experiments in which we neglect the influence of salinity on vertical  
148 mixing (as in e.g. Vialard and Delecluse, 1998). Section 2 describes the model, the observational  
149 datasets, the experimental design and the mixed layer temperature budget. Section 3 provides a  
150 validation of the simulated BoB climatological features, focusing on the key processes involved  
151 in Shenoi et al. (2002) hypothesis. Section 4 discusses the influence of salinity stratification on  
152 BoB climate, for both summer and winter. We will also show that our results are robust  
153 irrespective of whether we apply a flux correction or not to alleviate model biases, and for  
154 different choices of oceanic and atmospheric parameterizations. A summary and discussion of  
155 our results are finally presented in Section 5.

156

## 157 **2. Model and methods**

### 158 **2.1. Model configuration**

159 We use a regional coupled model to assess the influence of the BoB salinity stratification  
160 on the northern Indian Ocean climate. This model couples the NEMO (Nucleus for European  
161 Modelling of the Ocean) oceanic (Madec et al., 2008) and the WRF (Weather Research and  
162 Forecasting Model) atmospheric (Skamarock and Klemp, 2008) primitive equation models  
163 through the OASIS3 coupler (Valcke, 2013), and is named NOW for NEMO-OASIS-WRF.

164 We use a very similar Indian Ocean configuration to the one extensively described and  
165 validated in Samson et al. (2014), and therefore only provide a brief summary of this  
166 configuration in the following. This model is applied to the Indian Ocean sector (25.5°E-  
167 142.25°E, 34.5°S-26°N), with the oceanic and atmospheric component sharing the same  $1/4^\circ$  (~25  
168 km) horizontal grid. The ocean component has 46 vertical levels, with a resolution ranging from  
169 6 m to 18 m in the upper 100 m. The atmospheric component has 28 sigma vertical levels, with a  
170 higher resolution of 30 m near the surface. Variable lateral boundary conditions are supplied from  
171 a global simulation for the oceanic component (Brodeau et al., 2010), and from the ERA-Interim  
172 reanalysis (Dee et al., 2011) for the atmosphere. River runoffs are prescribed from the Dai and  
173 Trenberth (2002) climatological river product. This dataset includes the two major rivers flowing  
174 into the BoB (Ganges-Brahmaputra and Irrawady that collectively represent ~80% of the total  
175 river runoffs into the BoB) but also smaller rivers such as the Krishna, Godavari, and Mahanadi.



176 The ocean model parameterizations include a turbulent kinetic energy scheme for vertical  
177 mixing (Blanke and Delecluse, 1993). It uses a monochromatic formulation of the penetrative  
178 solar irradiance following a single exponential profile, with an e-folding depth scale set to 23 m  
179 corresponding to a Type I water in Jerlov's (1968) classification (oligotrophic waters). This  
180 parameterization is in line with recent observational estimates for the BoB (Lotliker et al., 2016).  
181 Atmospheric model physics include the Betts-Miller-Janjic (BMJ) scheme (Janjic, 1994) for  
182 subgrid-scale convection, the WRF single-moment six-class microphysics scheme WSM6 (Hong  
183 and Lim, 2006), the Dudhia (1989) shortwave radiation scheme, the Rapid Radiation Transfer  
184 Model (RRTM) for longwave radiation (Mlawer et al., 1997), the Yonsei University planetary  
185 boundary layer (Noh et al., 2003) and the four-layer Noah land surface model (Chen et al., 1996).

186 The present model setup differs from the simulations discussed in Samson et al. (2014) as  
187 the WRF model version has been updated from its version 3.2 to 3.3.1 and Dudhia (1989)  
188 shortwave radiation scheme has been preferred to the one of Goddard (Chou and Suarez, 1999).  
189 In line with the model version discussed in Samson et al. (2014), the reference simulation from  
190 the present configuration shares a lot in common with the one presented in Samson et al. (2014).  
191 Although an exhaustive validation of the present model configuration is out of the scope of this  
192 paper, a validation of the main model parameters involved in the feedback loop hypothesized by  
193 Shenoi et al. (2002) will be provided in Section 3.

## 194 **2.2. Experimental design**

195 The reference model simulation is referred to as the control run (CTL hereafter). This 18-  
196 year simulation was forced at the boundaries using conditions from the 1990-2007 period. The  
197 initial conditions on the 1<sup>st</sup> January 1990 are provided from ERA-Interim reanalysis data for the  
198 atmospheric component and from the  $\frac{1}{4}^\circ$  ocean simulation described in Brodeau et al. (2010) for  
199 the ocean. Additional sensitivity experiments were performed over the same period to test the  
200 impact of haline stratification on the BoB climate. They are listed in Table 1 and described  
201 below.

202 Vertical mixing is parameterized using a turbulent kinetic energy closure scheme (Blanke  
203 and Delecluse, 1993) in our CTL. Using a similar strategy to Vialard and Delecluse (1998) and  
204 Masson et al. (2005), we conduct a "NOS" sensitivity experiment. This experiment is identical to  
205 "CTL", except that the vertical mixing is resolved assuming a constant salinity of 35 pss in the  
206  $[5^\circ\text{S}-25^\circ\text{N}; 65^\circ\text{E}-105^\circ\text{E}]$  region (dashed blue frame on Fig. 3d) which encompasses the BoB and  
207 South-Eastern AS, where the seasonal export of BoB freshwaters induces a somewhat similar

208 behaviour to that in the BoB (e.g. de Boyer Montégut et al., 2007; Vinayachandran et al., 2007).  
209 The computation of vertical mixing is smoothly transitioned to fully accounting for the effects of  
210 salinity within  $5^\circ$  of the edges of this region. The NOS minus CTL experiment will thus  
211 specifically isolate effects of the salinity stratification in the BoB region on the regional climate,  
212 hence allowing to test the feedback loop hypothesized by Shenoi et al. (2002).

213 As we will see in more details in section 3, the CTL simulation strongly overestimates the  
214 wind stresses over the BoB, which yields a too deep mixed layer, too thin barrier layer and  
215 underestimated salinity stratification. Since the realism of the haline stratification is critical to our  
216 results, we performed a wind stress-corrected reference experiment FCTL (see Table 1), in which  
217 the wind stress provided to the ocean model was multiplied by a factor of 0.5 within the [ $8^\circ\text{N}$  -  
218  $26^\circ\text{N}$ ,  $76^\circ\text{E}$  - $100^\circ\text{E}$ ] region, with a smooth transition within  $6^\circ$  of the edges. Penetrative solar  
219 heat flux has a significant influence on the SST seasonal evolution in the BoB (e.g. de Boyer  
220 Montegut et al., 2007). We will demonstrate in section 3 that this flux correction approach  
221 strongly reduces the mixed layer depth (MLD) and barrier layer thickness (BLT) biases in the  
222 CTL experiment, and will further present our results based on FCTL and a twin experiment that  
223 neglects the effect of salinity stratification on vertical mixing (FNOS) in section 4. We will  
224 demonstrate in section 4 that our results are robust irrespective of whether the flux correction is  
225 applied or not.

226 Since our results could also be sensitive to some choices in physical parameterizations, we  
227 have also redone twin set of experiments similar to CTL and NOS with various choices. Howden  
228 and Murtugudde (2001) have shown that different SST anomalies develop in response to river  
229 inputs, depending on whether solar radiation is allowed to penetrate into the ocean or not. In  
230 order to test the sensitivity of our results to penetrative solar flux, we perform twin experiments  
231 for CTL and NOS, where the solar penetration is disabled and the entire solar flux is absorbed  
232 within the top model level (CTL\_NSP and NOS\_NSP experiments). Deep atmospheric  
233 convection is an essential component of Shenoi et al. (2002) hypothesis, and the results presented  
234 here may be sensitive to the convective scheme. The sensitivity of our results to the choice of  
235 convective scheme will thus be addressed by comparing results obtained using the BMJ moist  
236 convective adjustment scheme, with those obtained using the updated Kain-Fritsch (KF)  
237 atmospheric convective scheme (Kain, 2004) (CTL\_KF and NOS\_KF experiments). Similarly,  
238 the sensitivity of our results to the shortwave radiation scheme in experiments with the Goddard  
239 scheme (Chou and Suarez, 1999), previously employed in Samson et al. (2014) (CTL\_G and

240 NOS\_G experiments). As we will see, our results on the effect of the BoB haline stratification on  
 241 climatological rainfall are robust in any set of twin experiments above.

### 242 2.3. Mixed layer temperature budget.

243 The processes controlling SST are characterized using an online mixed layer heat budget  
 244 (Vialard and Delecluse, 1998; Vialard et al., 2001). The equation for the average temperature  
 245 over the time-varying mixed layer  $T_{ml}$  (a proxy for SST) reads as follows:

$$\begin{aligned}
 \partial T_{ml} = & -\frac{1}{h} \int_{-h}^0 u \partial_x T dz - \frac{1}{h} \int_{-h}^0 v \partial_y T dz - \frac{1}{h} \int_{-h}^0 D_l(T) \\
 & \text{horizontal advection} \qquad \qquad \qquad \text{lateral process} \\
 & -\frac{1}{h} (T_{ml} - T_{-h})(w_{-h} + \partial_t h) - \frac{1}{h} [K_z \partial_z T]_{-h} + \frac{Q_s(1-F_{-h}) + Q_{ns}}{\rho_0 C_p h} \qquad (1) \\
 & \text{subsurface vertical process} \qquad \qquad \qquad \text{atmospheric forcing}(F_T)
 \end{aligned}$$

247 The first two terms on the RHS respectively represent zonal and meridional temperature  
 248 advection in the mixed layer, where  $h$  is the time-varying model mixed layer estimated based on a  
 249 potential density increase of  $0.01 \text{ kg m}^{-3}$  relative to the density at 10-m depth and  $(u, v, w)$  are the  
 250 components of the current. The second term on the RHS represents lateral mixing processes,  
 251  $D_l(T)$  being model horizontal diffusion operator: this term will not be discussed in the following  
 252 as it is always negligible in the present analysis. The third term on the RHS gathers the vertical  
 253 exchanges of heat between the mixed layer and the subsurface ocean, including the effects of  
 254 upwelling  $w_{-h} (T_{-h} - T_{ml})$ , entrainment  $\partial_t h (T_{-h} - T_{ml})$  (computed as a residual from all the other  
 255 terms) and turbulent mixing at the bottom of the mixed layer  $K_z \partial_z T_{-h}$ , where  $K_z$  is the vertical  
 256 mixing coefficient for tracers. The last term on the RHS represents the atmospheric heat flux  
 257 forcing,  $Q_s$  and  $Q_{ns}$  being respectively the solar and non-solar components of the surface heat  
 258 flux,  $F_{-h}$  the fraction of incoming solar radiation that penetrates down to the depth  $h$ ,  $\rho_0$  the  
 259 seawater reference density, and  $C_p$  the sea water volumic heat capacity.

### 260 2.4. Validation datasets

261 The model SST and rainfall climatologies distribution are validated against the Tropical  
 262 Rainfall Measuring Mission (TRMM) Microwave Imager (TMI) dataset  
 263 (<http://www.remss.com/tmi>). The ERA-interim dataset (Dee et al., 2011) is used to validate the  
 264 wind at 10 m and air-sea heat and momentum fluxes are validated using the Tropflux product  
 265 (Praveen Kumar et al., 2012, 2013).

266 The ocean model climatological salinity and temperature distributions are validated against  
267 the North Indian Ocean Atlas (NIOA) (Chatterjee et al., 2012) dataset. The model MLD and BLT  
268 are compared with the observationally-derived climatology of de Boyer Montégut (2004)  
269 (<http://www.ifremer.fr/cerweb/deboyer/mld/home.php>). In order to be strictly comparable to this  
270 product, the model MLD and isothermal layer depth (ILD, with  $BLT=ILD-MLD$ ) are computed  
271 from 5-day averaged model temperature and salinity. We use the same criteria as in de Boyer  
272 Montégut (2004), i.e. a  $0.2^{\circ}\text{C}$  increase relative to 10-m depth temperature for ILD, and an  
273 equivalent density increase (on average  $0.065\text{ kg m}^{-3}$  for typical BoB temperature, salinity  
274 conditions) relative to 10-m depth density for MLD. The BLT estimate is anyway robust when  
275 computed with either the de Boyer Montégut (2004) criterion or the  $0.01\text{ kg.m}^{-3}$  criterion used for  
276 diagnosing the surface layer heat budget. Li et al. (2017) have found (their figure 5) that the BLT  
277 climatology diagnosed from the WOA13 dataset (which is similar to the NIOA atlas we use) is  
278 very similar to diagnosing this BLT from individual Argo profiles, suggesting that our approach  
279 for constructing our BLT validating dataset is reasonable.

### 280 **3. Model validation**

281 This section provides a brief validation of the reference (CTL) and flux-corrected (FCTL)  
282 simulations. The model climatology is always computed over the entire 18-years of the  
283 simulations. We will validate BoB-averaged climatologies of important parameters in the Shenoi  
284 et al. (2002) hypothesis, and demonstrate that the FCTL experiment compares better with  
285 observations. Finally, we will show the surface mixed layer heat budget in the FCTL experiment,  
286 which will allow to qualitatively check the consistency with previous studies.

#### 287 **3.1. Testing the validity of the wind stress correction approach**

288 Fig. 2 shows the climatological seasonal cycle of several BoB-averaged parameters that are  
289 important for testing Shenoi et al. (2002) hypothesis (SST, SSS, wind and wind stress, rainfall,  
290 net heat flux, haline stratification measured through MLD and BLT). Observationally-derived  
291 wind and wind stress are strongest during the southwest monsoon over the BoB, with a secondary  
292 maximum associated with the northeast monsoon in December-January (Fig. 2a,b). Rainfall is  
293 maximum in July during the southwest monsoon (Fig. 2c). Net air-sea heat fluxes into the ocean  
294 are largest before the monsoon, close to zero during the southwest monsoon, and become  
295 negative during the northeast monsoon (Fig. 2h). This seasonal heat flux evolution is generally  
296 consistent with the evolution of SST trend. SST is indeed warmest in the BoB in April-May

297 before the southwest monsoon (Fig. 2d) and coolest in January-February during the northeast  
298 monsoon. The strong monsoon rainfall (Fig. 2c) and river runoffs yield lowest salinities in  
299 October right after the southwest monsoon (Fig. 2e). The MLD has a clear semi-annual cycle  
300 with shallowest MLD during the inter-monsoon seasons, and deeper MLD during both monsoons  
301 (Fig. 2f), due to enhanced wind stirring (in summer) and negative air-sea fluxes (in winter). The  
302 barrier layer is thickest in boreal winter, i.e. after the southwest monsoon (Fig. 2g).

303 The control simulation generally reproduces the phase of the observed seasonal cycle quite  
304 well, but has several marked biases. First, the model wind stress is strongly overestimated all year  
305 long (by ~80% on average; see Fig. 2a). In contrast, the model wind speed is overestimated (by  
306 15% on average; see Fig. 2b). However, this overestimation also combines with a 20%  
307 overestimation of the wind variance (the June to September BoB-averaged CTL wind speed  
308 variance is  $4.5 \text{ m.s}^{-1}$  vs.  $3.7 \text{ m.s}^{-1}$  for ERA-I). The quadratic dependence of the wind stress on the  
309 wind velocity magnifies these two modest biases and results in a strong wind stress  
310 overestimation over the BoB. Rainfall is also overestimated by ~55% in summer over the BoB in  
311 the CTL experiment (Fig. 2c). Net heat flux into the ocean also exhibits a negative bias (Fig. 2h),  
312 larger from March to October ( $\sim 20 \text{ W.m}^{-2}$ ) mainly due an overestimated latent heat flux as a  
313 consequence of the overestimated wind speed (not shown). The net heat flux bias is in line with  
314 the  $\sim 1^\circ\text{C}$  too cold model SST (Fig. 2d). Despite the overestimated oceanic rainfall, the SSS is too  
315 salty (Fig. 2e) and the MLD too deep (Fig. 2f) all year-long in the CTL experiment. This is  
316 probably because the much too strong wind stress induces too much near-surface mixing. This  
317 intense wind stirring also yields a too thin barrier layer (Fig. 2g), especially in winter (the  
318 January-February average BLT is  $\sim 23 \text{ m}$  in CTL vs.  $\sim 35 \text{ m}$  in observations). The biases discussed  
319 above are of the same order or smaller than the ones in the previous coupled studies that tested  
320 the Shenoi et al. (2002) hypothesis.

321 We attempted to reduce those biases by applying an ad-hoc wind stress correction in the  
322 FCTL experiment. Fig. 2a shows that our strategy of the modifying wind stress is successful in  
323 producing a much more realistic wind stress seasonal cycle (Fig. 2a). It also considerably  
324 improves the haline stratification, confirming that the too strong wind stirring was the main cause  
325 of this bias. Applying the flux correction indeed results in a strong reduction of the MLD bias all  
326 through the year (Fig. 2f). It also corrects the salty SSS bias found in CTL, with SSS in FCTL  
327 that even becomes fresher than observations (Fig. 2e). The barrier layer bias is also reduced, with  
328 a thickness that is very close to observations in January-July and even overestimated by 5 to 10 m

329 from August to December. It must however be noted that this wind-stress correction has little  
330 impact on the rainfall (Fig. 2c) and SST (Fig. 2d) systematic biases, which already suggests a  
331 weak impact of salinity stratification on climatological SST and rainfall. This will be confirmed  
332 by all the set of twin experiments discussed later in the paper.

333 Given that FCTL exhibits a more realistic salinity stratification (although slightly  
334 overestimated) as compared to CTL, we will present results derived from this experiment in the  
335 rest of section 3 and in most of section 4. We will discuss the possible effect of FCTL remaining  
336 biases (too cold BoB, too strong rainfall, slightly overestimated haline stratification) on our  
337 results in section 5.

### 338 **3.2. Winter and summer simulated climate**

339 In this subsection, we will mainly focus on summer (June to September, hereafter JJAS)  
340 and winter (December to March, hereafter DJFM). Summer is the focus of Shenoi et al. (2002)  
341 and is characterized by the strongest BoB freshwater forcing. We will also discuss winter, for  
342 which salinity stratification impacts the BoB climate most in the only available regional coupled  
343 model study (Seo et al., 2009).

344 Despite the rainfall overestimation illustrated by Fig. 2c, the FCTL experiment generally  
345 reproduces the observed seasonal rainfall and wind climatologies (not shown). To quantify this,  
346 we compute pattern correlations discussed hereafter which were calculated with respect to the  
347 observational climatologies mentioned in section 2.4 for the northern Indian Ocean region ( $0^{\circ}$ -  
348  $25^{\circ}\text{N}$ ;  $40^{\circ}\text{E}$ - $100^{\circ}\text{E}$ ). This pattern correlation reaches 0.84 (summer) and 0.94 (winter) for rainfall  
349 and 0.93 (summer) and 0.92 (winter) for wind speed. The FCTL simulation also captures  
350 seasonal SST patterns very well (0.90 pattern correlation for summer and 0.93 for winter), despite  
351 the general tendency to underestimate the SST by about  $\sim 1^{\circ}\text{C}$  seen in Fig. 2d.

352 Fig. 3 provides a more thorough validation of the BoB SSS (colours) and BLT (a proxy for  
353 the vertical stratification, contours). The strong freshwater fluxes arising from the summer  
354 oceanic precipitation and continental runoffs result in a strong freshening (with SSS as low as 30  
355 pss) in the northern and eastern part of the BoB in summer (Fig. 3a), where river runoff and  
356 oceanic precipitation are most intense, with saltier waters to the south. During summer, barrier  
357 layer only develops in the eastern BoB (contours on Fig. 3a). During winter, the SSS distribution  
358 remains roughly consistent to that in in summer (with fresher water to the North), but with less  
359 intense meridional SSS gradients (Fig. 3b). In winter, observations indicate 20 to 30 m thick  
360 barrier layers develop in the northern BoB (contours on Fig. 3b) and expand into the southeastern

361 AS. The model reproduces the observed SSS patterns very well (a pattern correlation of 0.97 for  
362 JJAS and 0.98 for DJMF), with low salinity in the northern and eastern BoB and saltier water to  
363 the south and in the AS in both summer and winter. The model also qualitatively reproduces the  
364 observed barrier layer distribution (0.80 pattern correlation in summer and 0.81 in winter), with  
365 barrier layers mainly located in the eastern BoB in summer and thicker, more widespread barrier  
366 layers in the south-eastern AS and BoB in winter. It must however be noted that the model BLT  
367 is underestimated in the northern BoB in winter (up to 40 m in observations against 25 to 30 m in  
368 the model), which could be related to the model thermohaline biases in this region, whose  
369 possible impacts will be further discussed in section 5.2.

### 370 **3.3. Simulated seasonal upper-ocean heat balance**

371 To investigate the Shenoi et al. (2002) hypothesis with confidence, we need to assess  
372 whether the upper ocean thermal heat balance (that controls the SST) is qualitatively similar in  
373 our model to what was described from previous observational and modelling studies. Fig. 4  
374 provides the mean seasonal cycle of the mixed layer heat budget terms (described in section 2.3)  
375 averaged over the BoB, along with the MLD and surface net heat flux components.

376 From February to April, the total tendency is positive (Fig. 4a) and associated to rising SST  
377 before the monsoon (Fig. 2d). This heating tendency is driven by the positive net air-sea heat  
378 fluxes result from a combination of (1) increased shortwave radiation (Fig. 4b) due to the  
379 northward migration of the sun during spring and low nebulosity before the monsoon and (2)  
380 reduced latent heat fluxes (Fig. 4b) due to the mild winds at this time of the year (Fig. 2b). This  
381 warming by the atmospheric forcing is partially counterbalanced by vertical processes (Fig. 4a),  
382 which tend to cool the ocean surface by promoting mixing with deeper, cooler water. The  
383 advection terms are relatively weak when averaged over the entire BoB.

384 The SST first cools slightly at the beginning of the summer monsoon (May to July, Fig.  
385 2d). The initial cooling is largely the result of a strong decrease of the heating by atmospheric  
386 heat fluxes (Fig. 4a), which does not balance the cooling through vertical processes any more.  
387 The weaker warming by air-sea fluxes is due to both a reduction of incoming solar radiation (due  
388 to the strong nebulosity) and relatively strong latent heat fluxes (Fig. 4b) associated with the  
389 strong winds at this season (Fig. 2b). Towards the end of the monsoon (August to September),  
390 the warming tendency due to surface net heat fluxes is almost balanced by the cooling by vertical  
391 processes (Fig. 4a), and SST does not vary much in that period (Fig. 2d).

392 From October to January, the BoB cools (Fig. 2d and Fig. 4a). This cooling is driven by  
393 negative surface net heat fluxes (Fig. 4b) in response to reduced incoming solar radiation due to  
394 the southward migration of the sun and increased latent heat loss (Fig. 4b) due to northeast  
395 monsoon winds (Fig. 2b). The longwave fluxes also contribute to the negative net heat fluxes  
396 during winter months, because of a less humid atmosphere and weaker greenhouse effect. During  
397 that period, the mixed layer deepens (Fig. 2f) and oceanic vertical processes act to warm the  
398 surface layer and to damp the heat flux winter cooling (Fig. 4a). This warming by vertical mixing  
399 and entrainment of subsurface waters is due to the presence of temperature inversion during that  
400 season in the BoB in the model, as in observations (e.g. Thadatil et al., 2016).

401 This heat balance agrees qualitatively well with that presented from a forced model  
402 framework in figure 3c of de Boyer Montégut et al. (2007): the BoB SST changes are flux-driven  
403 with subsurface processes acting as a moderating factor. Both analyses also suggest a significant  
404 role of the haline stratification in maintaining relatively high SSTs in the BoB: during winter,  
405 vertical mixing and entrainment actually warm the surface layer due to the presence of a salinity-  
406 sustained temperature inversion.

407

#### 408 **4. Influence of salinity on Bay of Bengal Climatological Rainfall**

409 The analyses in section 3 suggest that the FCTL simulation captures the main  
410 climatological features of the northern Indian Ocean seasonal cycle for the key parameters  
411 involved in the Shenoi et al. (2002) hypothesis. The model in particular reproduces a warming  
412 tendency by oceanic vertical mixing and entrainment during winter, which could not happen in  
413 the absence of salinity stratification, and hence temperature inversion below the mixed layer. In  
414 the following subsections, we will first investigate how salinity influences exchanges of heat  
415 between the mixed layer and deeper ocean (section 4.1), before assessing its overall effect on  
416 climatological SST and rainfall (section 4.2). In section 4.3, we will demonstrate that the results  
417 obtained from the flux corrected experiments (FCTL and FNOS) are robust without the flux  
418 correction, and with several different choices of physical parameterisations.

##### 419 **4.1. Salinity reduces the vertical mixing of heat in the Bay of Bengal**

420 We first perform a consistency check to ascertain that the difference between FCTL and  
421 FNOS experiments indeed captures the expected oceanic impact of the salinity stratification. Fig.  
422 5a,c shows that the salinity stratification induces a shallower MLD everywhere in the BoB and



423 eastern AS. This salinity-induced MLD shoaling reaches 5.5 m in summer and 10.1 m in winter  
424 when averaged over the BoB. In the “NOS” experiments, the MLD is only sensitive to the  
425 thermal stratification, i.e. there is no barrier layer (Vialard and Delecluse, 1998). As expected, the  
426 salinity-induced MLD deepening pattern matches the barrier layer thickness pattern in the FCTL  
427 run, with largest ML deepening in regions where the barrier layers are thickest (contours on Fig.  
428 5). The pattern correlation between FNOS-FCTL MLD difference and FCTL BLT is indeed 0.86  
429 in JJAS and 0.95 in DJF. This analysis illustrates that the salinity effects assessed from FCTL  
430 minus FNOS are physically consistent.

431 Upper ocean salinity stratification strengthens the upper ocean stability in the BoB and  
432 eastern AS, and limits the downward mixing of heat. Fig. 5b,d shows the FCTL minus FNOS  
433 climatology of the mixed layer heating rate through vertical mixing (cf. equation 1). As expected,  
434 this difference is positive in regions where a barrier layer is present in FCTL. In regions where a  
435 temperature inversion is present, there is a warming by vertical processes in FCTL (cf section  
436 3.3), while there can only be a cooling by vertical processes in FNOS, where no temperature  
437 inversions can be sustained. In regions where no temperature inversion is present, the cooling by  
438 vertical processes is decreased in FCTL relative to FNOS, due to the insulating effect of the  
439 barrier layer. As a result, the salinity influence on vertical mixing always favours a warming of  
440 the mixed layer in regions where a barrier layer is present in FCTL (Fig. 5b,d). This salinity-  
441 induced warming through vertical mixing is not, in principle, only controlled by the barrier layer  
442 thickness distribution, but also by the salinity gradient across the barrier layer, temperature  
443 stratification below, and wind stirring. There is however an overall reasonable correspondence  
444 between the FCTL barrier layer thickness and salinity-induced change in turbulent heat fluxes at  
445 the bottom of the mixed layer, especially in winter (pattern correlation of 0.47 for JJAS and 0.81  
446 for DJFM).

447 Overall, the BoB salinity stratification inhibits vertical mixing, and contributes to a  
448  $+0.5^{\circ}\text{C}\cdot\text{month}^{-1}$  enhancement of the mixed layer heating rate by vertical mixing during JJAS and  
449  $+0.44^{\circ}\text{C}\cdot\text{month}^{-1}$  during DJFM. This impact of salinity stratification on the vertical mixing term  
450 is thus consistent with the Shenoi et al. (2002) hypothesis (Step II on Fig. 1) and other previous  
451 studies (de Boyer Montegut et al., 2007; Behara and Vinayachandran, 2016).

452 **4.2. Compensating effects yield a weak impact of salinity stratification on SST and**  
453 **rainfall**

454 Fig. 6 quantifies the climatological differences in BoB average SST and rainfall between  
 455 FNOS and FCTL. The simulated summer SST (Fig. 6a) and rainfall (Fig. 6b) climatologies are  
 456 almost identical in those simulations. Maps (not shown) likewise reveal very weak local rainfall,  
 457 wind and surface temperature changes, which are generally not statistically significant, including  
 458 on continents. In other words, the Shenoi et al. (2002) hypothesis does not seem to operate in our  
 459 model, i.e. the salinity stratification does not seem to influence the SST or rainfall climatology.  
 460 As we discussed above, however, salinity stratification contributes to an anomalous  $\sim 2^\circ\text{C}$  mixed  
 461 layer warming through vertical mixing over the summer monsoon (i.e.  $0.5^\circ\text{C}\cdot\text{month}^{-1}$  during 4  
 462 months). Our simulations are thus consistent with the step II of the Shenoi et al. (2002)  
 463 hypothesis on Fig. 1 (cf. Section 4.1). The absence of any significant climatological SST change  
 464 however indicates that other processes compensate the salinity-induced warming through vertical  
 465 mixing, yielding a weak impact on climatological SST (step III), and thus no impact on  
 466 freshwater forcing through ocean-atmosphere coupling (step I). In the rest of this subsection, we  
 467 will explain why there is no SST change despite the strong salinity-induced anomalous surface  
 468 warming by vertical mixing.

469 Fig. 7a shows the BoB-average FCTL minus FNOS mixed layer heat budget climatology,  
 470 i.e. the salinity contribution to the SST balance. In line with the analysis shown on Fig. 5c,d, the  
 471 salinity stratification contributes to a mixed layer warming through vertical mixing (blue curve  
 472 on Fig. 7a), in particular during and after the summer monsoon. However, this warming tendency  
 473 by subsurface processes is almost entirely balanced by a cooling tendency by atmospheric forcing  
 474 (orange curve on Fig. 7a). This almost equal compensation between the salinity-induced surface  
 475 layer heating by vertical mixing and cooling by atmospheric forcing results in an almost nil total  
 476 SST tendency (Fig. 7a) and therefore very similar SSTs in the FCTL and FNOS experiments  
 477 (Fig. 6a).

478 Several processes can lead to the change in the atmospheric forcing term seen on Fig. 7a.  
 479 This term reads as follows:

$$480 \quad \frac{Q_S(1-F_h)+Q_{NS}}{\rho_0 C_p h} \quad (2)$$

481 First, a change in one or several components of the surface heat flux (solar  $Q_S$  and non-solar  $Q_{NS}$   
 482 surface fluxes) can alter the net heat flux entering into the ocean and modulate the amplitude of  
 483 the atmospheric forcing term. Second, a change in the MLD impacts the atmospheric forcing  
 484 term by either modulating the heat capacity of the mixed layer ( $\rho_0 C_p h$  at the denominator of

485 equation 2) or by regulating the fraction of solar flux that penetrates below the mixed layer ( $F_h$  in  
486 equation 2). Fig. 7c allows estimating those effects separately. The red curve on Fig. 7c is an  
487 offline re-computation of FCTL minus FNOS term in equation (2). It does not match exactly the  
488 orange curve on Fig. 7a due to the offline computation with 5-day average rather than  
489 instantaneous values, but captures its general evolution. The blue curve on Fig. 7c shows this  
490 difference, but neglecting the effect of changes in surface fluxes (see Annex A for details). The  
491 orange curve neglects the effects of the mixed layer heat capacity changes, and the green curve  
492 those of solar penetration. When a coloured curve departs from the red curve, it indicates that  
493 salinity influences the heating rate of the mixed layer through that particular effect (see Annex A  
494 for details).

495 Fig. 7c shows that the influence of each of these effects is seasonally-dependent. For  
496 instance, there is a clear and dominant effect of salinity on the surface forcing heating rate  
497 through the mixed layer heat capacity from November to January (see yellow shading on Fig. 7c).  
498 In contrast, changes of surface fluxes contribute most to the atmospheric forcing change from  
499 March to October. Below, we will separately discuss the November to January (dominant effect  
500 of mixed layer heat capacity) and June to October (dominant effect of changes in air-sea fluxes)  
501 periods.

502 The barrier layer is thickest in the model (and observations) from November to February  
503 (Fig. 2g), and this is also the season when salinity contributes to the strongest shoaling of the  
504 mixed layer (Fig. 7b). Net surface heat fluxes are negative during this period (Fig. 2h) and  
505 contribute to cool the oceanic mixed layer (orange curve on Fig. 4a). By making the mixed layer  
506 shallower during this period, salinity reduces its heat capacity and allows a larger cooling rate in  
507 response to negative surface heat fluxes. During November to January, salinity thus does not  
508 change SST because the warming it induces through its effect on vertical mixing is compensated  
509 by a cooling due to negative surface heat fluxes being trapped over a shallower mixed layer.

510 During June to October, the salinity-induced anomalous cooling is dominated by the effect  
511 of a surface net heat flux reduction. Air-sea heat fluxes are indeed different in the FCTL and  
512 FNOS experiments (Fig. 7d), with latent heat fluxes dominating those differences during this  
513 period. A more detailed analysis (not shown) indicates that latent heat flux increases due to a  
514 slightly warmer SST and slightly stronger surface winds in the FCTL experiment. Although those  
515 mean SST and wind change are small, they are sufficient to explain the change in latent heat flux,  
516 because the Clausius-Clapeyron relation implies an exponential increase of the latent heat fluxes

517 with background SST, and hence a strong sensitivity of latent heat fluxes to those variables at the  
518 BoB high climatological SSTs. Overall, the slightly larger SST and winds in the FCTL  
519 simulation contribute to increase upward latent heat fluxes during and shortly after the southwest  
520 monsoon, largely cancelling the effect of salinity-induced warming by vertical processes.

### 521 **4.3. Robustness of the results**

522 Overall, the FCTL and FNOS experiments suggest that salinity stratification favours an  
523 anomalous warming of the surface layer through vertical mixing, but that this warming is  
524 compensated by a salinity-induced cooling of the surface layer by air-sea fluxes. As a result, the  
525 SST (and consequently the rainfall) hardly changes due to salinity stratification effects in the  
526 FNOS experiment. In this section, we will investigate the robustness of those results, by  
527 investigating the differences in BoB SST and rainfall climatological seasonal cycle in a series of  
528 twin-experiments similar to FTCL and FNOS, but no flux correction and different choices in  
529 terms of physical parameterizations (cf section 2.2).

530 Fig. 8a,b shows the mean seasonal cycle of the BoB SST and rainfall in the CTL and NOS  
531 experiments (i.e. as FCTL and FNOS, but without a flux correction). Although this experiment  
532 has a quite different mean state to the FCTL experiment, with a saltier SSS, deeper MLD and  
533 thinner BLT, there is also an almost negligible impact of salinity stratification on the BoB SST  
534 and rainfall in this experiment. Fig. 8c,d shows a similar experiment to CTL (i.e. with no flux  
535 correction), but where solar heat flux is not allowed to penetrate into the ocean, likewise yield  
536 almost no change in climatological SST and rainfall. This illustrates that ignoring solar  
537 penetration or considering it does not change the climatological SST or rainfall. Similarly,  
538 sensitivity experiments similar to CTL and NOS, but with a different shortwave radiative scheme  
539 (Fig. 8e,f) or convective parameterization (Fig. 8g,h) also suggest a very minor impact of the  
540 haline stratification on both SST and rainfall. Overall, our coupled model results are insensitive  
541 to whether or not we apply a flux correction, consider or not the penetration of solar heat flux, or  
542 to a change of the parameterization of two important atmospheric physical processes in the  
543 problem that we consider.

544

## 545 **5. Summary and discussion**

### 546 **5.1. Summary**

547 The monsoonal rains feed the northern BoB with a large quantity of freshwater, from  
548 oceanic rain and river runoffs. This results in some of the lowest surface salinities in the tropical  
549 band. Shenoi et al. (2002) proposed that the resulting very strong vertical salinity stratification is  
550 involved in a positive feedback loop that sustains intense rainfall in this region. This feedback  
551 loop would act as follows. The strong vertical salinity stratification inhibits the vertical mixing of  
552 heat. This contributes to maintaining SST above the  $\sim 28.5^{\circ}\text{C}$  threshold for deep atmospheric  
553 convection, hence contributing to intense rain above the BoB, which closes the positive feedback  
554 loop.

555 In the present paper, we explore the Shenoi et al. (2002) hypothesis in a 25-km resolution  
556 regional coupled climate model. An 18-year long reference experiment was run and validated.  
557 The model reproduces the main features of the northern Indian Ocean mean climate in both  
558 summer and winter, including the warming of the surface layer through vertical mixing  
559 associated with the thick barrier layer and temperature inversions during and after the monsoon.  
560 It however tends to produce 50% too strong wind stress, too deep mixed layer and too thin barrier  
561 layer when run without flux correction. We largely reduce those biases in a flux-corrected  
562 experiment where wind stress is artificially reduced over the BoB. We will discuss possible  
563 caveats associated with remaining model biases (in particular a 15% overestimation of wind  
564 speed and  $1^{\circ}\text{C}$  SST cold bias over the BoB) in section 5.2.

565 The role of salinity stratification is then evaluated in a sensitivity experiment in which  
566 vertical mixing is computed based on the thermal stratification only (i.e. the haline stratification  
567 is neglected). Differences between the wind-stress corrected control experiment and this  
568 sensitivity experiment allow evaluating the effect of salinity stratification on the northern Indian  
569 Ocean mean climate. Through the analysis of the surface layer heat budget, we find that salinity  
570 stratification indeed tends to warm the mixed layer through vertical mixing, during both summer  
571 and winter, as hypothesized by Shenoi et al. (2002). Based on observations, Shenoi et al. (2002)  
572 predicted an increase in SST and corresponding changes in precipitation related to this mixed  
573 layer warming. However, in our experiments, which resolve atmospheric feedbacks, salinity  
574 induces a compensating cooling through two distinct mechanisms. During early winter (from  
575 November to January), this salinity-induced cooling is of oceanic origin. Salinity indeed induces  
576 a thinner, lower heat-capacity mixed layer that cools more in response to the negative air-sea  
577 fluxes during this season. During late summer (from July to October), the salinity-enhanced  
578 cooling by surface heat-fluxes is dominated by changes in air-sea fluxes. During and shortly after

579 the southwest monsoon, salinity induces more heat losses through latent heat fluxes at the ocean  
580 surface, due to slightly warmer SST and stronger winds.

581 Because of these compensating effects on the upper ocean heat budget, salinity does not  
582 influence the BoB climatological SST and rainfall in our simulations. This result is very robust,  
583 as it is preserved in other sets of sensitivity experiments without the flux correction; without a  
584 penetration of solar heat fluxes into the ocean; and with a different parameterization of  
585 atmospheric convection or shortwave fluxes. In the next subsection, we discuss our results  
586 against previous studies, their robustness, and how they may be affected by model biases.

## 587 **5.2. Discussion**

588 Below, we will start by comparing our results with those of previous studies, for winter and  
589 summer. We will then discuss caveats of the present study.

590 Let us start by comparing our results with other studies for winter. In their 4-layers  
591 reduced-gravity model, Han et al. (2001) found little effect of neither rainfall nor river runoffs on  
592 the winter BoB SST. Howden and Murtugudde (2001) found an overall 0.5 to 1°C cooling of the  
593 Northern BoB in winter, in response to adding river runoffs, but this model has SSS biases of up  
594 to 3 pss relative to the Levitus climatology in winter (their plate 2). Behara and Vinayachandran  
595 (2016) also found that rivers led to an SST cooling during the entire year along the eastern and  
596 northern rim of the BoB, due to winter cooling by atmospheric fluxes projecting onto a thinner  
597 mixed layer. Seo et al. (2009) find a cooling over the entire northern BoB in their regional  
598 coupled model in winter due to the same process. The difference between our results and those of  
599 Seo et al. (2009) and Behara and Vinayachandran (2016) for winter SST arises from a different  
600 balance between two competing processes. Those two studies find, as we do, that salinity reduces  
601 the winter mixed layer depth, leading to a more efficient cooling by atmospheric fluxes. In  
602 contrast with those two studies, we find that – as hypothesized by Shenoi et al. (2002) – salinity  
603 stratification also reduces the vertical mixing of heat at the bottom of the mixed layer, with an  
604 overall negligible effect on the surface layer heat budget due to this compensation. While the  
605 studies by Han et al. (2001) and Howden and Murtugudde (2001) respectively suffered from a  
606 very simplified modelling framework and large biases, the last three studies have comparable  
607 resolutions, physical parameterizations and biases, making it difficult to conclude which one is  
608 the most realistic, and calling for more studies with other coupled models.

609 For summer, Han et al. (2001) found a weak impact of both rainfall and river runoffs on  
610 SST. Howden and Murtugudde (2001) found a very localised impact of the river runoff near the

611 Ganges-Brahmaputra mouth. We won't discuss Behara and Vinayachandran (2016), for which  
612 the influence of river runoff on summer SST is due to changes during winter. As in our case, Seo  
613 et al. (2009) found very little changes in SST and rainfall at the BoB scale during summer. We  
614 find a large impact of salinity on vertical mixing of heat as in several previous studies, but with  
615 little impact on SST due to a compensating change in air-sea fluxes. Except for Howden and  
616 Murtugudde (2001), there is therefore overall a stronger consensus about salinity not bringing  
617 any SST change in summer amongst previous studies although the underlying mechanisms may  
618 be different.

619 Let us now discuss some caveats of our study. With  $\frac{1}{4}$  degree grid spacing, our ocean  
620 model is eddy-permitting but not eddy-resolving. This may be an issue, because the BoB has a  
621 relatively strong eddy kinetic energy (EKE; e.g. Chelton et al., 2011) generated from remote  
622 wind forcing and ocean internal instability (Chen et al., 2018), and eddy may contribute to the  
623 SST balance through their influence on upper ocean heat transport. Comparison with altimeter  
624 estimates (not shown) however indicate a reasonable representation of the EKE in the BoB, with  
625 an underestimation of less than 15%.

626 Despite the fact to the model used in the present study is amongst one of the best state-of-  
627 the-art coupled models for its representation of the northern Indian Ocean climate (Samson et al.,  
628 2014) or when compared to the study of Seo et al. (2009), it is not exempt from biases. Even the  
629 flux-corrected experiment tends to have a too low surface salinity due to too strong rainfall (Fig.  
630 2c,e) and a  $\sim 1^\circ\text{C}$  too cool SST all year long (Fig. 2d). Let us briefly discuss the impact of those  
631 biases. As displayed on Fig. 9, the salinity stratification is overestimated in FCTL and  
632 underestimated in CTL as compared to observationally-derived climatologies, yet the two  
633 experiments give similar results (no impact of this salinity stratification on the climatological  
634 SST and rainfall), suggesting that this bias has little impact on our results. Observed SSS  
635 climatologies however generally underestimate the northern BoB freshening because of the  
636 scarcity of salinity measurements in this region as suggested by the very fresh surface signals  
637 reported by recent measurements from moored buoys (Sengupta et al., 2016; Wijesekera et al.,  
638 2016) and satellite observations (Fournier et al., 2017). Validating the model vertical salinity  
639 profile to the northernmost RAMA mooring in the BoB ( $15^\circ\text{N}$ ) indeed suggest that FCTL  
640 exhibits a small surface salty bias SSS and a deeper than observed halocline (Fig. 9). Both  
641 experiments also tend to underestimate the temperature stratification below  $\sim 50$  m. These biases

642 of temperature and salinity profiles could result in an underestimation of the effect of salinity on  
643 the vertical turbulent heat fluxes.

644 There is a  $\sim 1^\circ\text{C}$  cold SST bias in our model setup (Fig. 2d). This bias is partly related to  
645 the 15% wind speed overestimation in the BoB (Fig. 2b), which leads to an overestimated  
646 evaporative cooling. This  $\sim 1^\circ\text{C}$  cold bias could significantly impact our results. In observations,  
647 SST is above the observed  $28.5^\circ\text{C}$  threshold for deep atmospheric convection (dashed line on Fig.  
648 2d) from March to November, and is very close to this threshold in July-September, implying a  
649 strong sensitivity to a potential small SST change. In contrast, the model is below this threshold  
650 from July to March (i.e. during most of the southwest monsoon). Figure 10 compares the relation  
651 between daily SST and rainfall over the BoB in the model and observations. Observed rainfall is  
652 most likely at  $\sim 29^\circ\text{C}$ , with a large increase of strong rainfall rates occurrence between  $28^\circ\text{C}$  and  
653  $29^\circ\text{C}$ . In the model, this “switch” to the convective regime occurs at lower SST, between 27 and  
654  $28^\circ\text{C}$ . i.e. the model has a  $1^\circ\text{C}$  cold SST bias, but its convective threshold is also  $1^\circ\text{C}$  cooler than  
655 in observations. For this reason, we believe that the cold bias over the BoB in the model does not  
656 strongly affect our results.

657

### 658 **Acknowledgements**

659 The authors thank IFCPAR (Indo French Centre for Promotion of Advanced Research),  
660 New Delhi for funding of the 4907-1 proposal, CNES for funding the SeaLevelALK proposal  
661 and the LEFE/EC2CO program for funding of the AO2015-873251 proposal. The simulations  
662 used in this study were performed on resources provided by PRACE Research Infrastructure  
663 resources CURIE at TGCC, France. We also thank IRD (Institut de Recherche pour  
664 le Developpement) for the financial support of the Indo-French collaboration on Indian  
665 Ocean research. This is NIO contribution number XXXX.

666



667 **Annex A: processes responsible for the change in the effect of atmospheric heat fluxes**

668

669 The heating rate of the mixed layer by atmospheric heat flux forcing reads as follows:

$$\frac{Q_S(1 - \mathcal{F}_{-h}) + Q_{NS}}{\rho_0 C_P h} \quad (a)$$

670 The red curve on fig.7c shows the difference between this term in the control experiment

671 (designated by a c superscript) and “NOS” experiment (designated by a n superscript):

$$\Delta = \frac{Q_S^c(1 - \mathcal{F}_{-h^c}) + Q_{NS}^c}{\rho_0 C_P h^c} - \frac{Q_S^n(1 - \mathcal{F}_{-h^n}) + Q_{NS}^n}{\rho_0 C_P h^n} \quad (b)$$

672 This term can become large due to several processes. First, a change in one or several

673 components of the surface heat flux can alter the net heat flux entering into the ocean (solar  $Q_s$ 674 and non-solar  $Q_{ns}$  surface fluxes) and modulate the amplitude of the atmospheric forcing term.675 This effect can be evaluated by comparing  $\Delta$  to the term  $\Delta_{flux}$  below:

$$\Delta_{flux} = \frac{Q_S^c(1 - \mathcal{F}_{-h^c}) + Q_{NS}^c}{\rho_0 C_P h^c} - \frac{Q_S^n(1 - \mathcal{F}_{-h^n}) + Q_{NS}^n}{\rho_0 C_P h^n} \quad (c)$$

676 The computation above neglects changes in  $Q_S$  and  $Q_{NS}$ . When  $\Delta$  is different from  $\Delta_{flux}$ , it means

677 that the contribution of changes in fluxes matter. A similar strategy is used to identify the effects

678 of two other processes. A change in the MLD  $h$  impacts the atmospheric forcing term in two679 ways. On the one hand, it modulates the heat capacity of the mixed layer  $\rho_0 C_P h$  at the

680 denominator of equation (2): a thicker mixed layer is for example less responsive to a given heat

681 flux. This effect is identified by comparing  $\Delta$  to the term  $\Delta_{hc}$  below:

$$\Delta_{hc} = \frac{Q_S^c(1 - \mathcal{F}_{-h^c}) + Q_{NS}^c}{\rho_0 C_P h^c} - \frac{Q_S^n(1 - \mathcal{F}_{-h^n}) + Q_{NS}^n}{\rho_0 C_P h^n} \quad (d)$$

682 On the other hand, the MLD modulates the fraction of solar flux that penetrates below the mixed

683 layer ( $\mathcal{F}_{-h}$  of last term in equation 1): a thicker mixed layer intercepts more of the incoming solar684 heat flux (i.e.  $1 - \mathcal{F}_{-h}$  is larger) than a thin mixed layer. This effect is identified by comparing  $\Delta$  to685 the term  $\Delta_{sp}$  below:

$$\Delta_{sp} = \frac{Q_S^c(1 - \mathcal{F}_{-h^c}) + Q_{NS}^c}{\rho_0 C_P h^c} - \frac{Q_S^n(1 - \mathcal{F}_{-h^n}) + Q_{NS}^n}{\rho_0 C_P h^n} \quad (e)$$

686 Fig. 7c shows the seasonal climatology of  $\Delta$ ,  $\Delta_{flux}$ ,  $\Delta_{hc}$ , and  $\Delta_{sp}$ .

687 **References**

- 688 Akhil, V.P., Durand, F., Lengaigne, M., Vialard, J., Keerthi, M.G., Gopalakrishna, V.V., Deltel,  
689 C., Papa, F., de Boyer Montégut, C., 2014. A modeling study of the processes of surface  
690 salinity seasonal cycle in the Bay of Bengal. *J. Geophys. Res. Oceans* 119, 3926-3947.  
691 doi:10.1002/2013JC009632.
- 692 Behara, A., Vinayachandran, P.N., 2016. An OGCM study of the impact of rain and river water  
693 forcing on the Bay of Bengal. *J. Geophys. Res. Oceans* 121, 2425-2446.  
694 doi:10.1002/2015JC011325.
- 695 Blanke, B., Delecluse, P., 1993. Variability of the tropical Atlantic Ocean simulated by a general  
696 circulation model with two different mixed-layer physics. *J. Phys. Oceanogr.* 23(7), 1363-  
697 1388. doi:10.1175/1520-0485(1993)023<1363:VOTTAO>2.0.CO;2.
- 698 Brodeau, L., Barnier, B., Treguier, A.M., Penduff, T., Gulev, S., 2010. An ERA40-based  
699 atmospheric forcing for global ocean circulation models. *Ocean. Model.* 31(3-4), 88-104.  
700 doi:10.1016/j.ocemod.2009.10.005.
- 701 Chaitanya, V.S., Lengaigne, M., Vialard, J., Gopalakrishna, V.V., Durand, F., Kranthikumar, C.,  
702 Amritash, S., Suneel, V., Papa, F., Ravichandran, M., 2014. Salinity Measurements  
703 Collected by Fishermen Reveal a “River in the Sea” Flowing Along the Eastern Coast of  
704 India. *Bull. Am. Meteorol. Soc.* 95, 1897-1908. doi:10.1175/BAMS-D-12-00243.1.
- 705 Chatterjee, A., Shankar, D., Shenoi, SSC., Reddy, G.V., Michael, G.S., Ravichandran, M.,  
706 Gopalkrishna, V.V., Rama Rao, E.P., Udaya Bhaskar, T.V.S., Sanjeevan, V.N., 2012. A  
707 new atlas of temperature and salinity for the north Indian Ocean. *J. Earth. Syst. Sci.* 121(3),  
708 559-593.
- 709 Chelton, D.B., Schlax, M.G., Samelson, R.M., 2011. Global observations of nonlinear mesoscale  
710 eddies, *Prog. Oceanogr.*, 91, 167–216, doi:10.1016/j.pcean.2011.01.002.
- 711 Chen, F., Mitchell, K., Schaake, J., Xue, Y., Pan, H-L., Koren, V., Duan, Q.Y., Ek, M., Betts, A.,  
712 1996. Modeling of land surface evaporation by four schemes and comparison with FIFE  
713 observations. *J. Geophys. Res.* 101(D3), 7251-7268. doi:10.1029/95JD02165.
- 714 Chen, G., Li, Y., Xie, Q., Wang, D., 2018. Origins of eddy kinetic energy in the Bay of Bengal. *J.*  
715 *Geophys. Res. Ocean.* 123, 2097-2115. <https://doi.org/10.1002/2017JC013455>
- 716 Chou, M-D., Suarez, M.J., 1999. A solar radiation parameterization (CLIRAD-SW) developed at  
717 Goddard Climate and Radiation Branch for Atmospheric Studies, Goddard Space Flight  
718 Center, Greenbelt, NASA Tech. Memo. NASA/TM-1999-104606(15).

- 719 Dai, A., Trenberth, K.E., 2002. Estimates of freshwater discharge from continents: Latitudinal  
720 and seasonal variations. *J. Hydrometeorol.* 3, 660-687.
- 721 de Boyer Montégut, C., Madec, G., Fischer, A.S., Lazar, A., Iudicone, D., 2004. Mixed layer  
722 depth over the global ocean: an examination of profile data and a profile-based climatology.  
723 *J. Geophys. Res.* 109, C12003. doi:10.1029/2004JC002378.
- 724 de Boyer Montégut, C., Vialard, J., Shenoi, S.S.C., Shankar, D., Durand, F., Ethé, C., Madec, G.,  
725 2007. Simulated Seasonal and Interannual Variability of the Mixed Layer Heat Budget in  
726 the Northern Indian Ocean. *J. Climate* 20(13), 3249-3268. doi:10.1175/JCLI4148.1.
- 727 Dee, D.P., et al., 2011. The ERA-Interim reanalysis: Configuration and performance of the data  
728 assimilation system. *Q J Roy Meteorol Soc* 137(656), 553-597. doi:10.1002/qj.828.
- 729 Dudhia, J., 1989. Numerical study of convection observed during the Winter Monsoon  
730 Experiment using a mesoscale two-dimensional model. *J. Atmos. Sci.* 46, 3077-3107.
- 731 Durack, P.J., Wijffels, S.E., 2010. Fifty-year trends in global ocean salinities and their  
732 relationship to broad-scale warming. *J. Climate* 23(16), 4342-4362.
- 733 Findlater, J., 1969. A major low-level air current near the Indian Ocean during the northern  
734 summer. *Q. J. Roy. Meteorol. Soc.* 95, 362-380. doi: 10.1002/qj.49709540409.
- 735 Fournier, S.J., Vialard, J., Lengaigne, M., Lee, T., Gierach, M.M., Chaitanya, A.V.S., 2017.  
736 Unprecedented satellite synoptic views of the Bay of Bengal “river in the sea”. *J. Geophys.*  
737 *Res. Ocean*, online first, doi: 10.1002/2017JC013333.
- 738 Gadgil, S., Gadgil, S., 2006. The Indian Monsoon, GDP and Agriculture. *Economic and Political*  
739 *Weekly* 41(47), 4887-4895.
- 740 Gadgil, S., Joshi, N.V., Joseph, P.V., 1984. Ocean-atmosphere coupling over monsoon regions.  
741 *Nature.* 312, 141-143.
- 742 Girishkumar, M.S., Ravichandran, M., McPhaden, M.J., 2013. Temperature inversions and their  
743 influence on the mixed layer heat budget during the winters of 2006–2007 and 2007–2008  
744 in the Bay of Bengal. *J. Geophys. Res.* 118, 2426-2437. doi: 10.1002/jgrc.20192.
- 745 Graham, N.E., Barnett, T.P., 1987. Sea surface temperature, surface wind divergence and  
746 convection over tropical oceans. *Science.* 238, 657-659. doi:10.1126/science.238.4827.657.
- 747 Han, W., McCreary, J.P., Kohler, K.E., 2001. Influence of precipitation minus evaporation and  
748 Bay of Bengal rivers on dynamics, thermodynamics, and mixed layer physics in the upper  
749 Indian Ocean. *J. Geophys. Res.* 106(C4),6895-6916. doi:10.1029/2000JC000403.

- 750 Held, I.M., Soden, B.J., 2006. Robust responses of the hydrological cycle to global warming. *J.*  
751 *Climate* 19, 5686-5699.
- 752 Hong, S.Y., Lim, J.O.J., 2006. The WRF Single-Moment 6-Class Microphysics Scheme (WSM6)  
753 *J. Korean Meteor. Soc.* 42, 129-151.
- 754 Howden, S.D., Murtugudde, R., 2001. Effects of river inputs into the Bay of Bengal. *J. Geophys.*  
755 *Res.* 106(C9), 19825-19843. doi:10.1029/2000JC000656.
- 756 Janjić, Z.I., 1994. The step-mountain Eta coordinate model: Further developments of the  
757 convection, viscous sublayer, and turbulence closure schemes. *Mon. Weather Rev.* 122(5),  
758 927-945. doi:10.1175/1520-0493(1994)122<0927:TSMECM>2.0.CO;2.
- 759 Jerlov, N.G., 1968. *Optical oceanography*. Elsevier, London
- 760 Joseph, P.V., Raman, P.L., 1966. Existence of low level westerly jet-stream over peninsular India  
761 during July. *Indian J. Meteorol. Geophys.* 17, 407-410.
- 762 Kain, J.S., 2004. The Kain-Fritsch convective parameterization: an update. *J. Appl. Meteorol.* 43,  
763 170-181.
- 764 Kumari, A., Prasanna Kumar, S., Chakraborty, A., 2018. Seasonal and Interannual Variability in  
765 the Barrier Layer of the Bay of Bengal. *J. Geophys. Res. Oceans* 123, 1001–1015.  
766 <https://doi.org/10.1002/2017JC013213>.
- 767 Li, C., Yanai, M., 1996. The onset and interannual variability of the Asian summer monsoon in  
768 relation to land-sea thermal contrast. *J. Climate* 9, 358-375.
- 769 Li, Y., Han, W., Ravichandran, M., Wang, W., Shinoda, T., Lee, T., 2017. Bay of Bengal salinity  
770 stratification and Indian summer monsoon intraseasonal oscillation: 1. Intraseasonal  
771 variability and causes, *J. Geophys. Res. Oceans* 122, 4291-4311, doi:  
772 10.1002/2017JC012691.
- 773 Lotliker, A.A., Omand, M.M., Lucas, A.J., Laney, S.R., Mahadevan, A., Ravichandran, M.,  
774 2016. Penetrative radiative flux in the Bay of Bengal. *Oceanography* 29, 214-221.
- 775 Lukas, R., Lindstrom, E., 1991. The mixed layer of the western equatorial Pacific Ocean *J.*  
776 *Geophys. Res.* 96(S01), 3343-3357. doi:10.1029/90JC01951.
- 777 Madec, G., 2008. NEMO ocean engine, Note du Pôle de modélisation, Institut Pierre-Simon  
778 Laplace (IPSL), France, No 27, ISSN No 1288-1619, 2008.
- 779 Masson, S., et al., 2005. Impact of barrier layer on winter–spring variability of the southeastern  
780 Arabian Sea. *Geophys. Res. Lett.* 32, L07703. doi:10.1029/2004GL021980p.

- 781 Mignot, J., de Boyer Montégut, C., Lazar, A., Cravatte, S., 2007. Control of salinity on the mixed  
782 layer depth in the world ocean: 2. Tropical areas, *J. Geophys. Res.* 112, C10010.  
783 doi:10.1029/2006JC003954.
- 784 Mlawer, E.J., Taubman, S.J., Brown, P.D., Iacono, M.J., Clough, S.A., 1997. Radiative transfer  
785 for inhomogeneous atmospheres: RRTM, a validated correlated-k model for the longwave,  
786 *J. Geophys. Res.* 102(D14), 16663-16682. doi:10.1029/97JD00237.
- 787 Noh, Y., Cheon, W.G., Hong, S.Y., Raasch, S., 2003. Improvement of the K-profile model for  
788 the planetary boundary layer based on large eddy simulation data. *Bound. Lay. Meteorol.*  
789 107(2), 401-427. doi:10.1023/A:1022146015946.
- 790 Praveen Kumar, B., Vialard, J., Lengaigne, M., Murty, V., McPhaden, M., 2012. Tropflux: air-  
791 sea fluxes for the global tropical oceans—description and evaluation. *Clim. Dyn.* 38, 1521-  
792 1543. doi:10.1007/s00382-011-1115-0.
- 793 Praveen Kumar, B., Vialard, J., Lengaigne, M., Murty, V., McPhaden, M., Cronin, M., Pinsard,  
794 F., Reddy, K.G., 2013. Tropflux wind stresses over the tropical oceans: Evaluation and  
795 comparison with other products. *Clim. Dyn.* 40, 2049. <https://doi.org/10.1007/s00382-012-1455-4>.
- 797 Rao, R.R., Sivakumar, R., 2003. Seasonal variability of sea surface salinity and salt budget of the  
798 mixed layer of the north Indian Ocean, *J. Geophys. Res.* 108(C1), 3009.  
799 doi:10.1029/2001JC000907.
- 800 Samson, G., Masson, S., Lengaigne, M., Keerthi, M.G., Vialard, J., Pous, S., Madec, G.,  
801 Jourdain, N.C., Jullien, S., Menkes, C., Marchesiello, P., 2014. The NOW regional coupled  
802 model: Application to the tropical Indian Ocean climate and tropical cyclone activity. *J.*  
803 *Adv. Model. Earth Syst.* 6, 700-722. doi:10.1002/2014MS000324.
- 804 Sengupta, D., Bharath Raj, G.N., Shenoi, S.S.C., 2006. Surface freshwater from Bay of Bengal  
805 runoff and Indonesian throughflow in the tropical Indian Ocean. *Geophys. Res. Lett.* 33,  
806 L22609. doi:10.1029/2006GL027573.
- 807 Sengupta, D., Bharath Raj, N., Ravichandran, M., Sree Lekha, J., Papa, F., 2016. Near-surface  
808 salinity and stratification in the north Bay of Bengal from moored observations. *Geophys.*  
809 *Res. Lett.* 43, 4448-4456. doi:10.1002/2016GL068339.
- 810 Seo, H., Xie, S., Murtugudde, R., Jochum, M., Miller, A.J., 2009. Seasonal effects of Indian  
811 Ocean freshwater forcing in a regional coupled model. *J. Climate* 22, 6577-6596.

- 812 Shenoi, S.S.C., Shankar, D., Shetye, S.R., 2002. Differences in heat budgets of the near-surface  
813 Arabian Sea and Bay of Bengal: Implications for the summer monsoon. *J. Geophys. Res.*  
814 107(C6), 1-14.
- 815 Skamarock, W.C., Klemp, J.B., 2008. A Time-Split Nonhydrostatic Atmospheric Model for  
816 Weather and Forecasting Applications. *J. Comp. Phys.* 227, 3465-3485,  
817 doi:10.1016/j.jcp.2007.01.037.
- 818 Sprintall, J., Tomczak, M., 1992. Evidence of the barrier layer in the surface layer of the tropics,  
819 *J. Geophys. Res.* 97(C5), 7305-7316.
- 820 Thadathil, P., Muraleedharan, P.M., Rao, R.R., Somayajulu, Y.K., Reddy, G.V.,  
821 Revichandran, C., 2007. Observed seasonal variability of barrier layer in the Bay of  
822 Bengal, *J. Geophys. Res.* 112, C02009, doi:10.1029/2006JC003651.
- 823 Thadathil, P., Suresh, I., Gautham, S., Prasanna Kumar, S., Lengaigne, M., Rao, R.R., Neetu, S.,  
824 Hegde, A., 2016. Surface layer temperature inversion in the Bay of Bengal: Main  
825 characteristics and related mechanisms. *J. Geophys. Res. Oceans* 121, 5682-5696,  
826 doi:10.1002/2016JC011674.
- 827 Valcke, S., 2013. The OASIS3 coupler: A European climate modelling community software,  
828 *Geosci. Model. Dev.* 6(2), 373-388, doi:10.5194/gmd-6-373-2013.
- 829 Vialard, J., Delecluse, P., 1998. An OGCM Study for the TOGA Decade. Part I: Role of Salinity  
830 in the Physics of the Western Pacific Fresh Pool. *J. Phys. Oceanogr.* 28(6), 1071-1088.  
831 doi:10.1175/1520-0485(1998)028<1071:AOSFTT>2.0.CO;2.
- 832 Vialard, J., Menkes, C., Boulanger J.P., Delecluse P., Guilyardi, E., McPhaden, M.J., Madec, G.,  
833 2001. A model study of oceanic mechanisms affecting equatorial Pacific sea surface  
834 temperature during the 1997-98 El Niño. *J. Phys. Oceanogr.* 31(7), 1649-1675.
- 835 Vinayachandran, P.N., Jahfer, S., Nanjundiah, R.S., 2015. Impact of river runoff into the ocean  
836 on Indian summer monsoon. *Environ. Res. Lett.* 10(5), 054008. doi:10.1088/1748-  
837 9326/10/5/054008.
- 838 Vinayachandran, P.N., Murty, V.S.N., Ramesh Babu, V., 2002. Observations of barrier layer  
839 formation in the Bay of Bengal during summer monsoon. *J. Geophys. Res.* 107(C12), 8018,  
840 doi:10.1029/2001JC000831.
- 841 Vinayachandran, P.N., Shankar, D., Kurian, J., Durand, F., Shenoi, S.S.C., 2007. Arabian Sea  
842 mini warm pool and the monsoon onset vortex. *Current Sci.* 93(2), 203-214.
- 843 Webster, P.J., Magana, V.O., Palmer, T.N., Shukla, J., Tomas, R.A., Yanai, M., Yasunari, T.,

844 1998. Monsoons: Processes, predictability and prospects for prediction. *J. Geophys. Res.*  
845 103 (C7), 14451-14510.

846 Wijesekera, H.W., et al., (2016) ASIRI: an ocean–atmosphere initiative for Bay of Bengal. *Bull.*  
847 *Am. Meteorol. Soc.* 97(10), 1859-1884.

848

849

850

851

ACCEPTED MANUSCRIPT

852  
853  
854

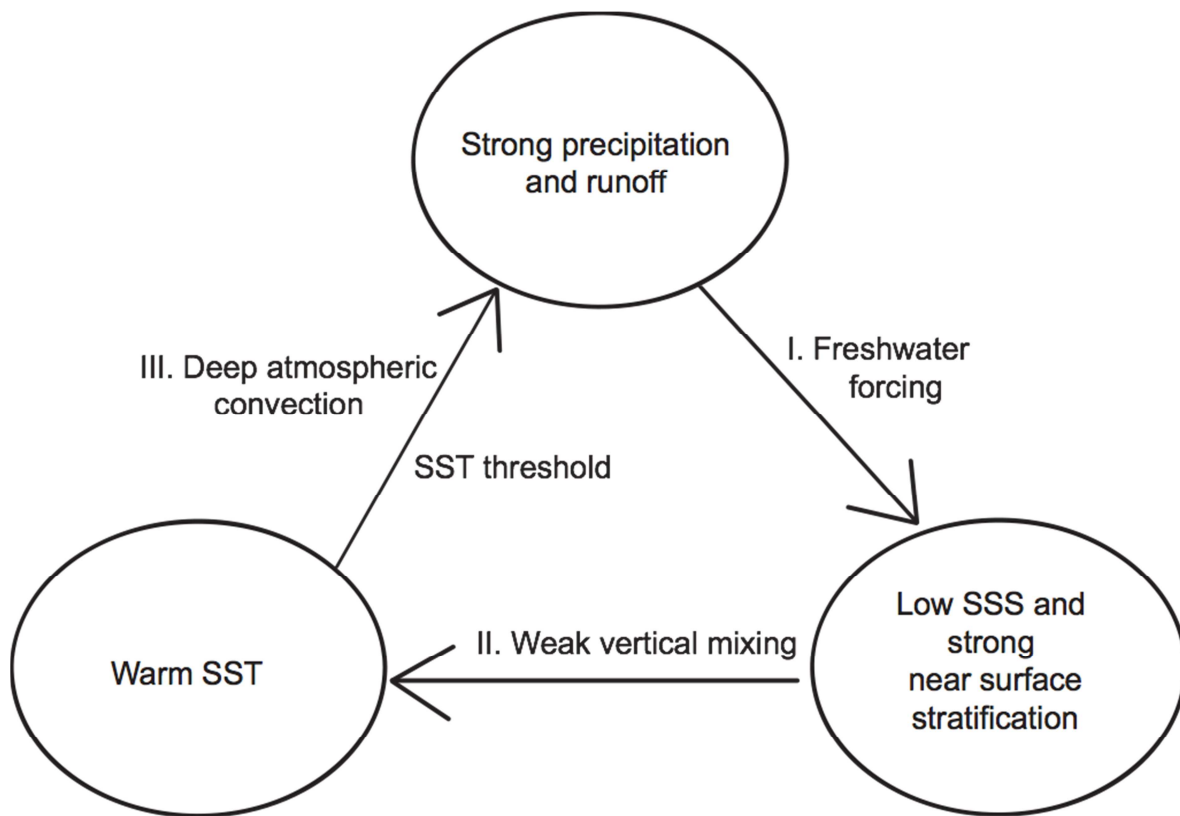
Experiment name	Purpose
CTL	Reference experiment. See text for details on resolution & configuration.
NOS	As CTL but with no impact of salinity on vertical mixing.
FCTL	As CTL, but with wind stress correction over the Bay of Bengal.
FNOS	As FCTL, but with no impact of salinity on vertical mixing.
CTL-NSP	As CTL, but with no solar flux penetration into the ocean.
NOS-NSP	As CTL_NSP, but with no impact of salinity on vertical mixing.
CTL-G	As CTL, but using Goddard shortwave radiation scheme.
NOS-G	As NOS, but using Goddard shortwave radiation scheme.
CTL-KF	As CTL, but using Kain-Fritsch sub-grid atmospheric convection scheme.
NOS-KF	As NOS, but using Kain-Fritsch sub-grid atmospheric convection scheme.

855

856 **Table 1:** NOW (NEMO-Oasis-WRF) regional coupled model experiments used in this study.

857  
858  
859  
860



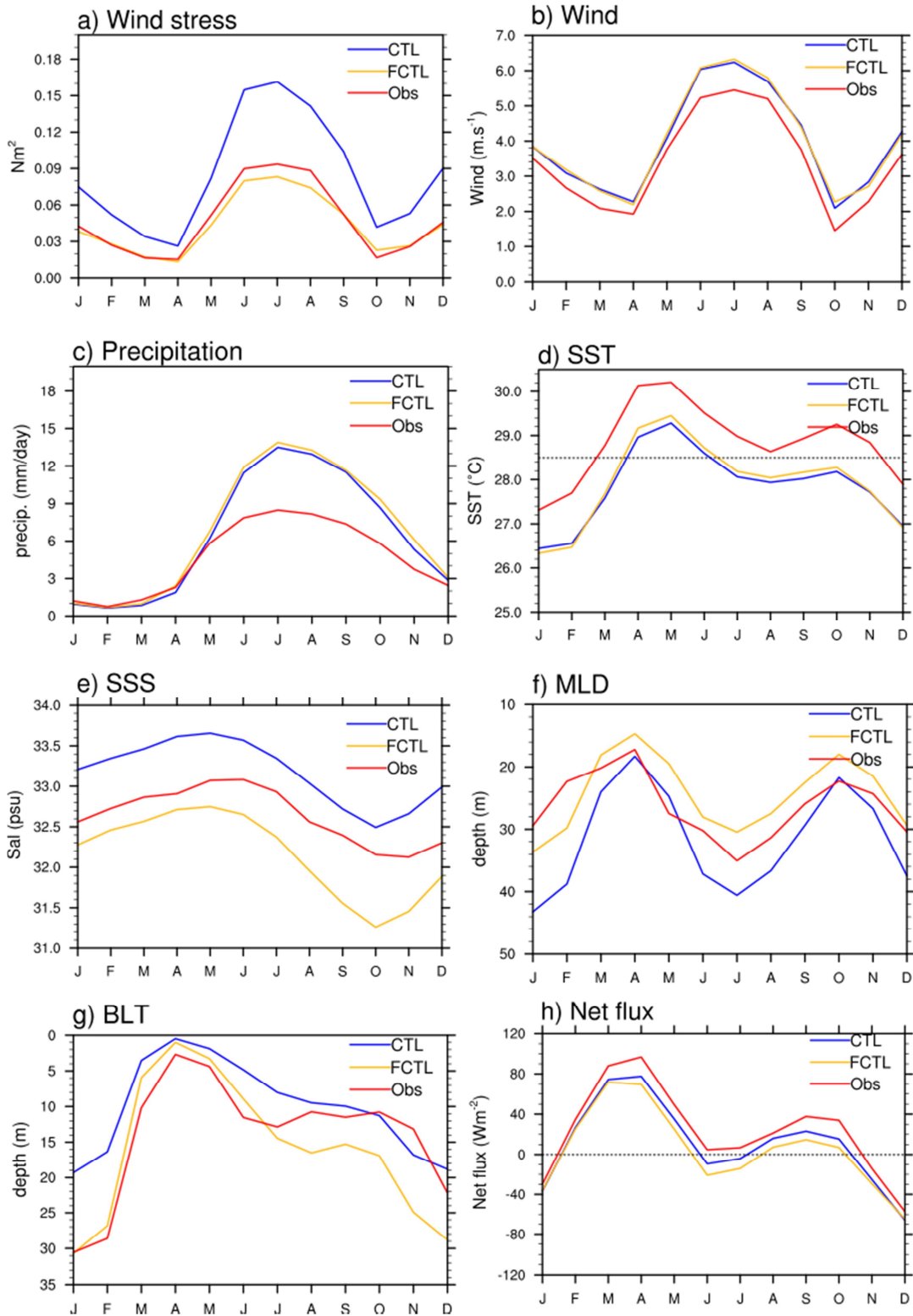


861

862 **Figure 1:** Sketch of the positive feedback mechanism proposed by Shenoi et al. (2002), by which  
863 the BoB haline stratification could sustain enhanced regional precipitation.

864

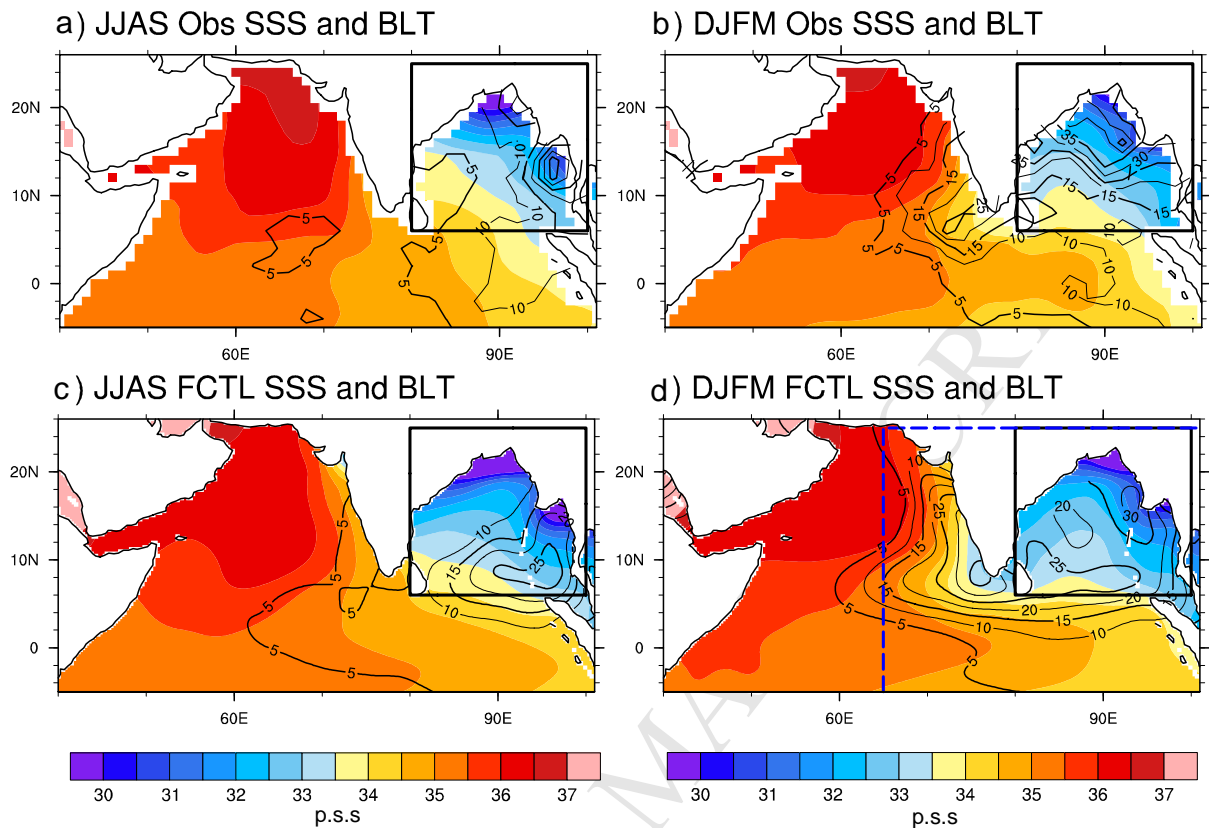
865



866

867 **Fig. 2** Averaged BoB (6°N-25°N, 80°E-100°E, see region on Fig. 3) climatological seasonal  
868 cycle for CTL (Blue) & FCTL (flux correction applied on wind stress: see text for details,  
869 yellow) experiments and observations (red) for (a) wind stress ( $\text{N.m}^{-2}$ ), (b) wind speed ( $\text{m.s}^{-1}$ ) (c)  
870 precipitation ( $\text{mm.day}^{-1}$ ) ( $\text{W.m}^{-2}$ ), (d) Sea Surface Temperature (SST, °C), (e) Sea Surface  
871 Salinity (SSS, pss), (f) mixed layer depth (MLD, m) (g) Barrier Layer Thickness (BLT, m) and  
872 (h) net heat flux. Observed climatologies are obtained from the TropFlux 1990-2007 average for  
873 wind stress and net heat flux, ERA-interim 1990-2007 average for wind speed, TMI 1998-2006  
874 average for SST, TRMM 1998-2011 average for rainfall, NIOA climatology for SSS and de  
875 Boyer Montegut et al. (2004) climatology for MLD and BLT. The dashed horizontal line on  
876 panel d indicates the observed threshold (28.5°C) for deep atmospheric convection.

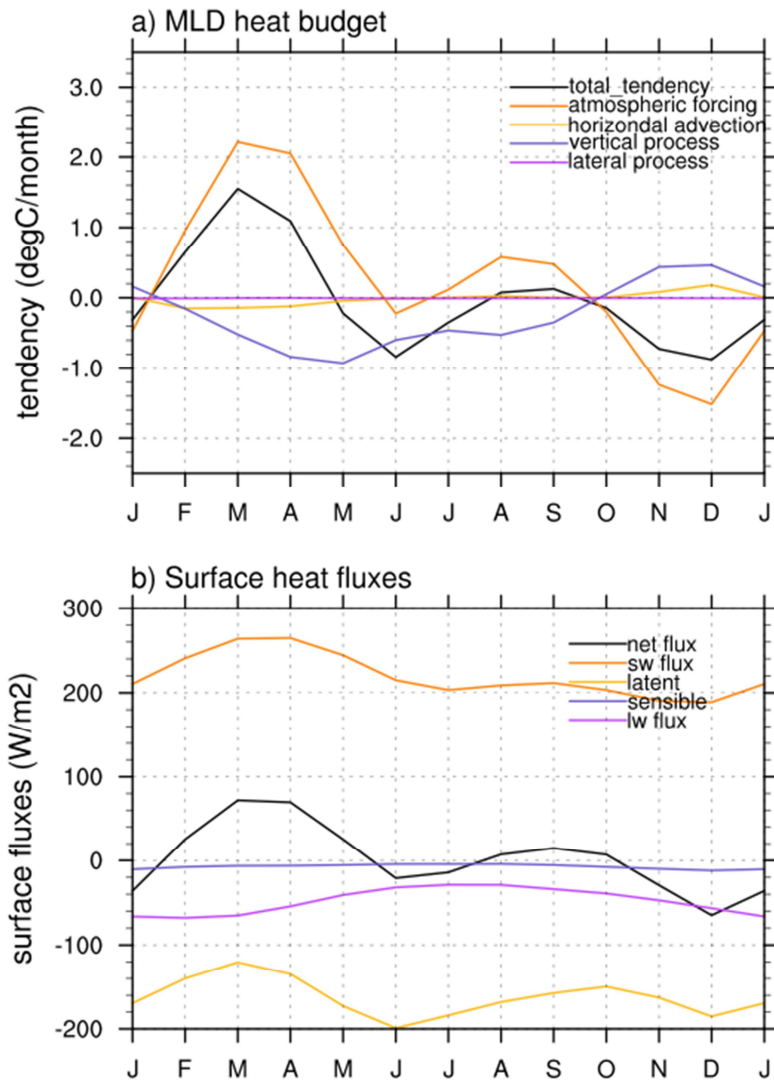
877



878

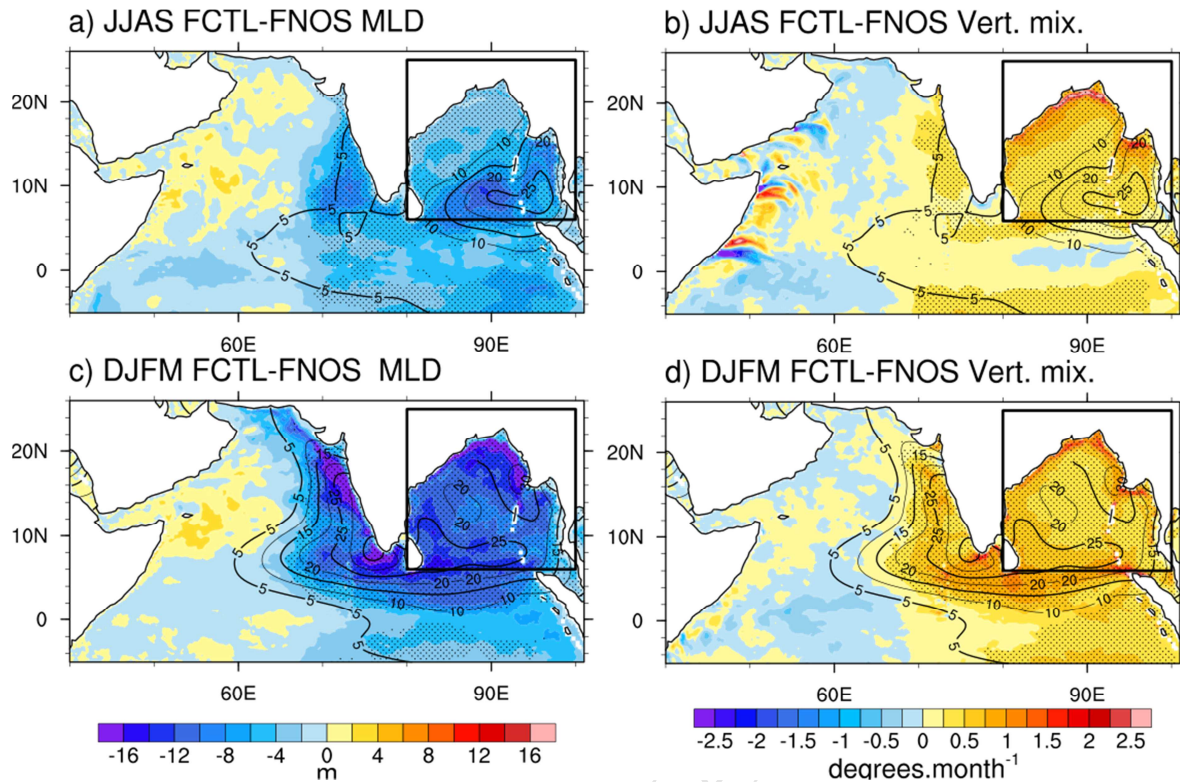
879 **Fig. 3** Summer (June to September: JJAS) (**left**) and Winter (December to March; DJFM) (**right**)  
 880 climatologies of observation (**top**) and FCTL (**bottom**) Sea Surface Salinity (SSS, shading, pss)  
 881 and Barrier Layer Thickness (BLT, contours, meters). For the model data, a horizontal smoothing  
 882 has been applied, with a similar spatial scale than that used for the observationally-derived  
 883 climatologies i.e. with a smoothing radius of 175 km for BLT as for de Boyer Montegut et al.  
 884 (2004) and 4° (444 km) for SSS as for the NIOA climatology. The dashed blue frame on panel d  
 885 indicates the region over which the influence of salinity on vertical mixing is neglected in the  
 886 series of “NOS” experiments (see table 1).

887



888

889 **Figure 4.** Averaged BoB climatological seasonal cycle of FCTL (a) mixed layer heat budget  
 890 terms ( $^{\circ}\text{C}\cdot\text{month}^{-1}$ , see section 2.3 for details) and (b) surface net heat fluxes and its four  
 891 components ( $\text{W}\cdot\text{m}^{-2}$ ).

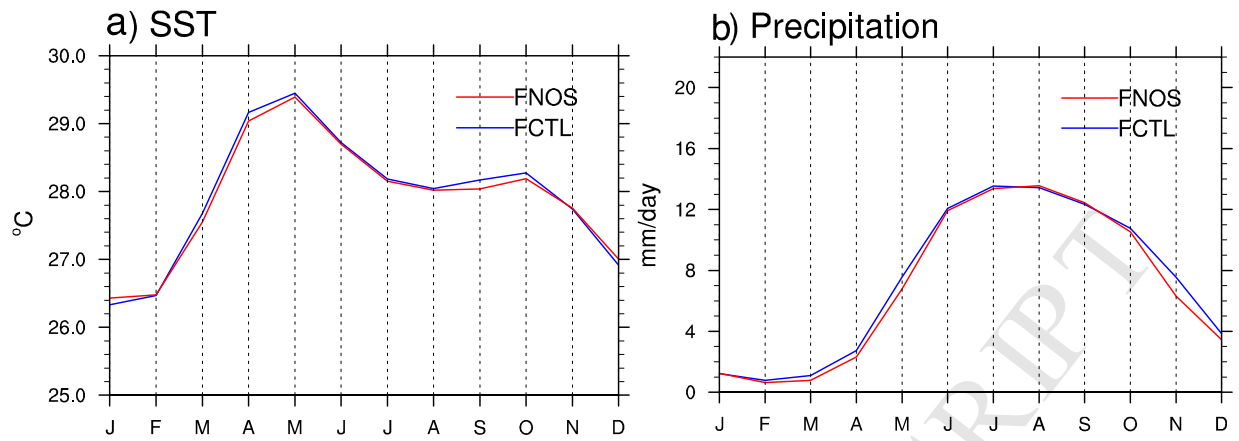


892

893 **Figure 5. (Top)** Summer (JJAS) and **(bottom)** winter (DJFM) climatological maps of FCTL  
 894 minus FNOS **(left)** mixed layer depth (m) and **(right)** vertical mixing term of the mixed layer  
 895 heat budget ( $^{\circ}\text{C}\cdot\text{month}^{-1}$ ). The FCTL run climatological barrier layer thickness is overlaid as  
 896 contours. Dots indicate regions for which MLD (left) and vertical mixing (right) differences  
 897 between the FCTL and FNOS simulations are significantly different from zero at the 95%  
 898 confidence level (using a one-tailed student's t-test with degrees of freedom equal to number of  
 899 years minus one).

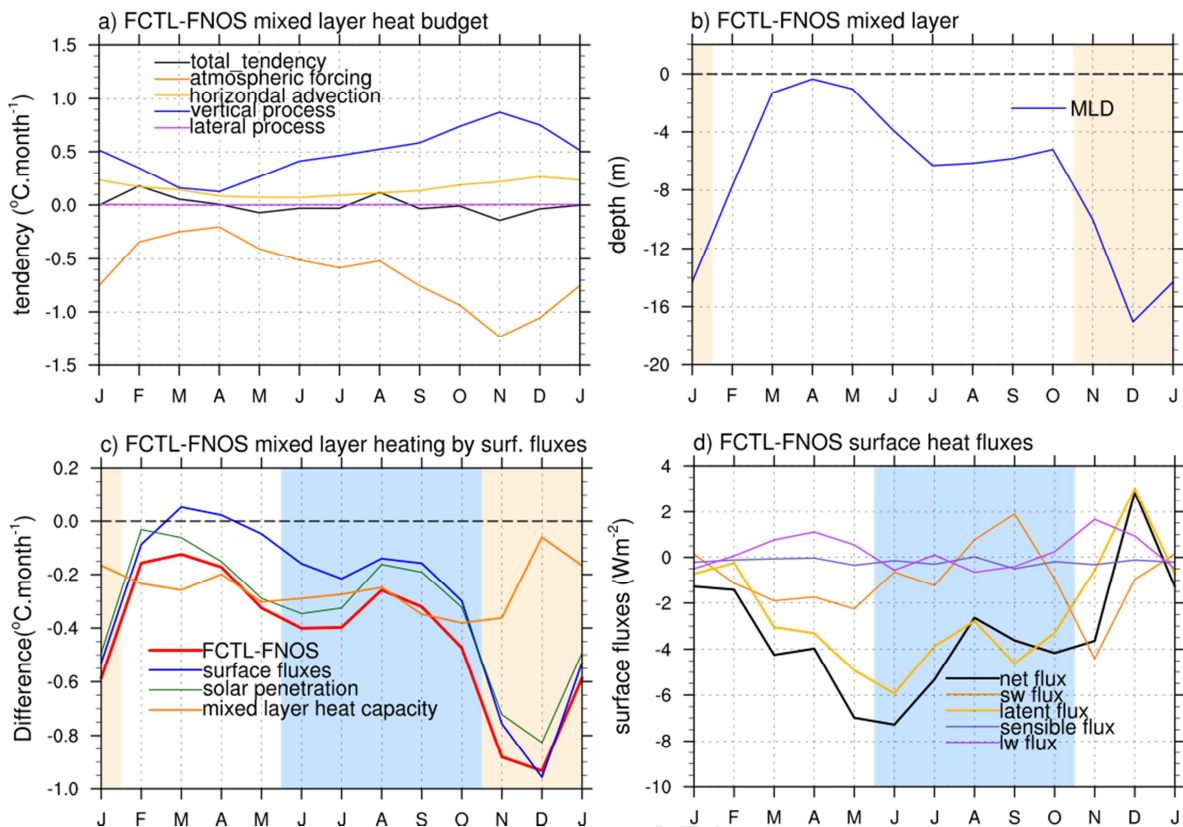
900

901



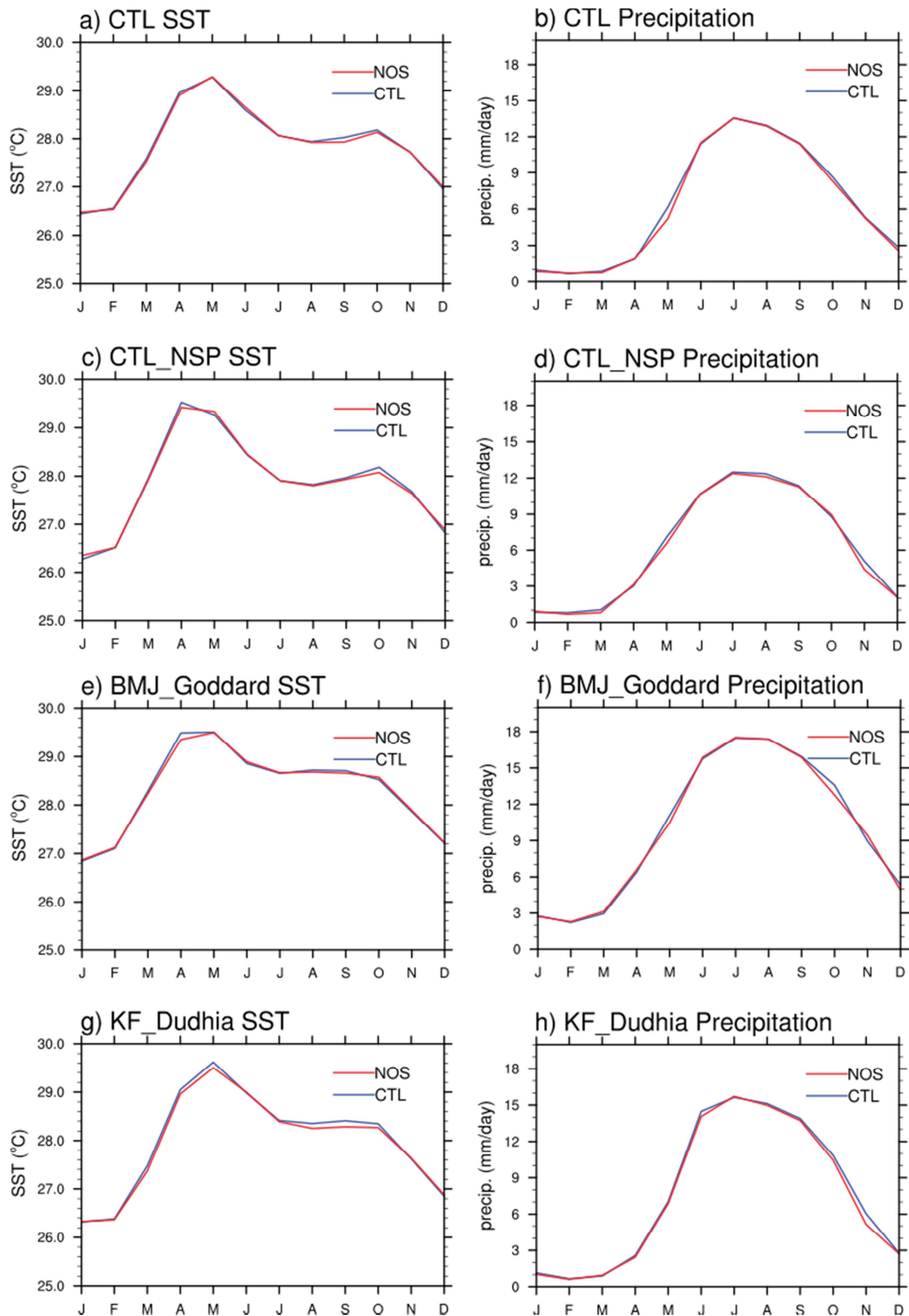
902

903 **Figure 6.** Average BoB FCTL and FNOS (e) SST and (f) precipitation climatological seasonal  
904 cycle.



905  
 906 **Figure 7.** Average BoB climatological seasonal cycle of FCTL minus FNOS (a) MLD heat  
 907 budget ( $^{\circ}\text{C}\cdot\text{month}^{-1}$ ), (b) MLD (m) and (d) surface fluxes ( $\text{W}\cdot\text{m}^{-2}$ ). (c) shows the FCTL minus  
 908 FNOS recomputed atmospheric forcing term (thick red curve). The green curve allows to  
 909 evaluate the effect of solar penetration, the blue curve the effect of the change in surface heat  
 910 fluxes and the orange one the effect of the changes in mixed layer heat capacity (see text and  
 911 Annex A for details). The blue shading highlights the July to October period and the salmon  
 912 shading highlights the November to January period.



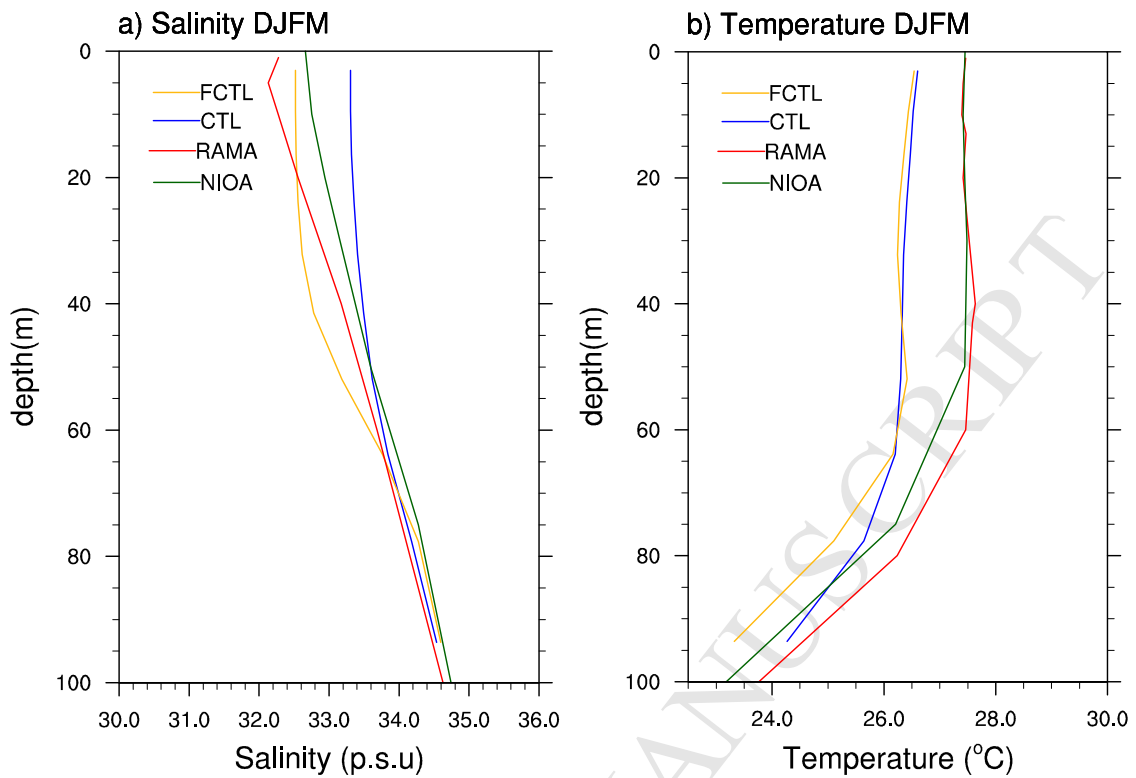


913

914 **Fig. 8:** Averaged BoB CTL and NOS mean seasonal cycle of (a) SST and (b) precipitation (i.e.  
 915 same as 8ef but without flux corrections). (c)-(d) Same as (a)-(b), but for CTL-NSP and NOS-  
 916 NSP (i.e. with the penetration of solar radiation into the ocean de-activated). (e)-(f) Same as (a)-

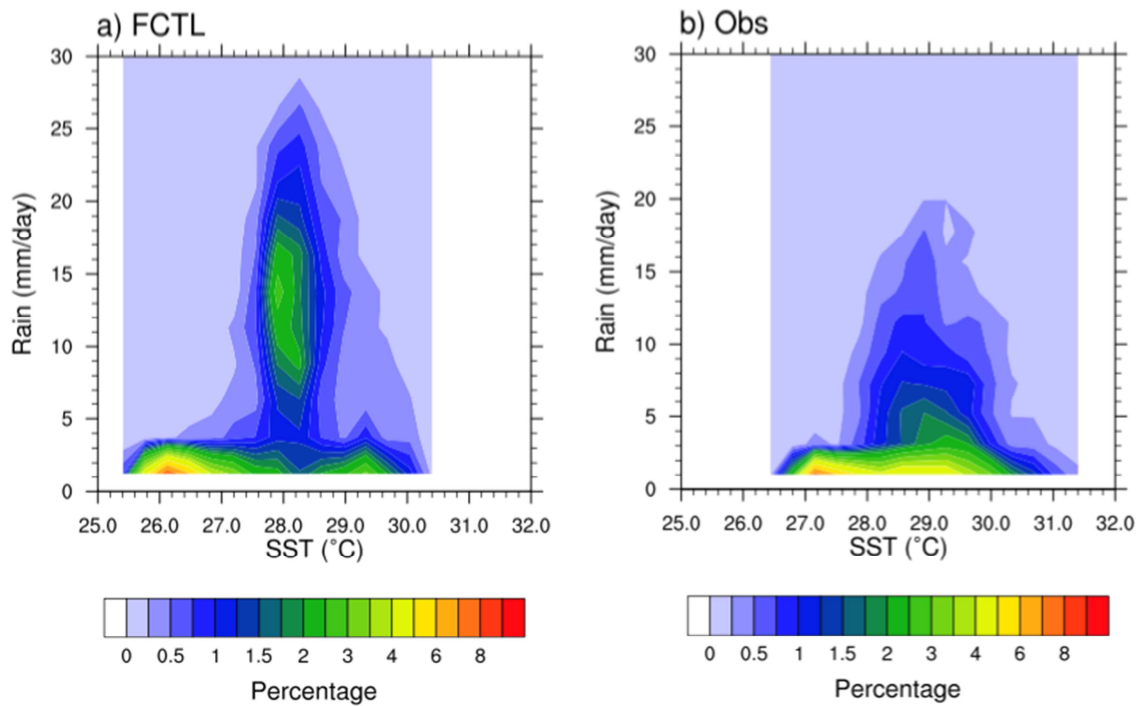
- 917 **(b)**, but for CTL-G and NOS-G (Goddard shortwave radiation parameterization). **(g)-(h)** Same as  
918 **(a)-(b)**, but for CTL-KF and NOS-KF (Kain-Fritsch convective parameterization).

ACCEPTED MANUSCRIPT



919

920 **Fig 9.** Winter (DJFM) temperature and salinity BoB-averaged climatological profiles for  
921 longitude 90°E and latitude 15°N from the RAMA buoy (red), NIOA product (green), CTL (blue)  
922 and FCTL (yellow).



923

924 **Figure 10:** SST-rainfall relation in (a) the FCTL simulation and (b) from TMI and TRMM  
925 observations. The probability density function (%) was constructed from daily SST and rainfall  
926 over the BoB region, using  $2.5 \text{ mm}\cdot\text{day}^{-1}$  and  $0.33^\circ\text{C}$  wide bins.